arXiv:1610.08108v1 [math.AP] 25 Oct 2016

PATTERN FORMATION OF A NONLOCAL, ANISOTROPIC INTERACTION MODEL

MARTIN BURGER, BERTRAM DÜRING, LISA MARIA KREUSSER, PETER A. MARKOWICH AND CAROLA-BIBIANE SCHÖNLIEB

Abstract. We consider a class of interacting particle models with anisotropic repulsive-attractive interaction forces whose orientations depend on an underlying tensor field. This class of models can be regarded as a generalisation of a gradient flow of a nonlocal interaction potential which has a local repulsion and a long-range attraction structure. The so-called Kücken-Champod model describing the formation of fingerprint patterns is an example of this class of models. We study the equilibria of the corresponding mean-field partial differential equation analytically and investigate pattern formation numerically in two dimensions.

1. Introduction

Nonlocal interaction models are mathematical models describing the collective behaviour of large numbers of individuals where each individual can interact not only with its close neighbours but also with individuals far away. These models serve as basis for biological aggregation and have given us many tools to understand the fundamental behaviour of collective motion and pattern formation in nature. For instance, these mathematical models are used to explain the complex phenomena observed in swarms of insects, flocks of birds, schools of fish or colonies of bacteria [17, 18, 39, 20, 7, 58, 57, 36, 44, 63, 48, 37, 13, 40, 14, 54, 16, 15, 29, 60].

One of the key features of many of these models is the social communication between individuals at different scales which can be described by short- and long-range interactions [7, 54, 40]. Over large distances the individuals in these models can sense each other via sight, sound, smell, vibrations or other signals. While most models consider only isotropic interactions, pattern formation in nature is often anisotropic [6] and an anisotropy in the communication between individuals is essential to describe these phenomena accurately. By adding an anisotropy to the simplified isotropic interaction model the resulting interaction model can be regarded as a generalisation of the isotropic interaction model. This more complex mathematical model captures many important swarming behaviours which are neglected in the simplified isotropic interaction model, including anisotropic pattern formation.

Isotropic interaction models with radial interaction potentials can be regarded as the simplest form of interaction models [4]. The resulting patterns are found as stationary points of the N particle interaction energy

$$E(x_1, \dots, x_N) = \frac{1}{2N^2} \sum_{\substack{j,k=1 \\ k \neq j}}^{N} W(x_j - x_k) \tag{1.1}$$

where $W(d) = w(|d|)$ denotes the radially symmetric interaction potential and $x_j = x_j(t) \in \mathbb{R}^n$ for $j = 1, \dots, N$ denote the positions of the particles at time $t \geqslant 0$ [13, 48]. The associated gradient flow is:

$$\frac{\mathrm{d}x_j}{\mathrm{d}t} = \frac{1}{N} \sum_{\substack{k=1 \\ k \neq j}}^{N} F(x_j - x_k) \tag{1.2}$$

where $F(d) = -\nabla W(d)$. Here, $F(x_j - x_k)$ is a conservative force, aligned along the distance vector $x_j - x_k$. The continuum equation corresponding to 1.2, also referred to as the aggregation

equation [9, 48, 13, 52], is given by

$$\rho_t + \nabla \cdot (\rho u) = 0, \qquad u = -\nabla W * \rho \tag{1.3}$$

where $\rho = \rho(t,x)$ is the density of particles at location $x \in \mathbb{R}^n$ and at time $t > 0$ and $u = u(t,x)$ is the macroscopic velocity field. The aggregation equation (1.3) has extensively been studied recently, mainly in terms of its gradient flow structure [53, 34, 62, 2, 22], the blow-up dynamics for fully attractive potentials [9, 26, 12, 33], and the rich variety of steady states [42, 43, 7, 59, 27, 32, 12, 4, 3, 64, 63, 5, 21, 25].

If the radially symmetric potential W is purely attractive, e.g. w is an increasing function with $w(0) = 0$, the density of the particles converges to a Dirac Delta function located at the center of mass of the density [19]. In this case, the Dirac Delta function is the unique stable steady state and a global attractor [26]. Under certain conditions the collapse toward the Dirac Delta function can take place in finite time [26, 9, 8, 11].

In biological applications, however, it is not sufficient to consider purely attractive potentials since the inherently nonlocal interactions between the individual entities occur on different scales [7, 40, 54]. These interactions are usually described by short-range repulsion to prevent collisions between the individuals as well as long-range attraction that keeps the swarm cohesive [55, 56]. The associated radially symmetric potentials w, also referred to as repulsive-attractive potentials, first decrease and then increase as a function of the radius. These potentials lead to possibly more complex steady states than the purely attractive potentials and can be considered as a minimal model for pattern formation in large systems of individuals [4].

The 1D nonlocal interaction equation with a repulsive-attractive potential has been studied in [43, 59, 42]. The authors show that the behaviour of the solution strongly depends on the regularity of the interaction potential. More precisely, the solution converges to a sum of Dirac masses for regular interaction, while it remains uniformly bounded for singular repulsive potentials.

Pattern formation for repulsive-attractive potentials in multi-dimensions is studied in [13, 63, 48]. The authors perform a linear stability analysis of ring equilibria and derive conditions on the potential to classify the different instabilities. This analysis can also be used to study the stability of flock solutions and mill rings in the associated second-order model [1]. A numerical study of the N particle interaction model for specific repulsion-attraction potentials [48, 13] outlines a wide range of radially symmetric patterns such as rings, annuli and uniform circular patches, while exceedingly complex patterns are also possible. The convergence of radially symmetric solutions toward spherical shell stationary states in multi-dimensions is discussed in [4]. Moreover, the nonlocal interaction equation in heterogeneous environments (where domain boundaries are also allowed) is investigated in [65].

Nonlocal interaction models have been studied for specific types of repulsive-attractive potentials [3, 28, 31, 24, 30, 44]. In [3] the dimensionality of the patterns is analysed for repulsive-attractive potentials that are strongly or mildly repulsive at the origin, i.e. potentials with a singular Laplacian at the origin satisfying $\Delta W(d) \sim -|d|^{-\beta}$ as $d \to 0$ for some $0 < \beta < n$ in n dimensions and potentials whose Laplacian does not blow up at the origin satisfying $W(d) \sim -|d|^{\alpha}$ as $d \to 0$ for some $\alpha > 2$, respectively. In [44] a specific example of a repulsive-attractive potential is studied, given by a Newtonian potential for the repulsive and a polynomial for the attractive part, respectively.

In this work, we consider an evolutionary particle model with an anisotropic interaction force. More precisely, we generalise the extensively studied model (1.2) by considering an N particle model of the form

$$\frac{\mathrm{d}x_j}{\mathrm{d}t} = \frac{1}{N} \sum_{\substack{k=1 \\ k \neq j}}^{N} F(x_j - x_k, T(x_j)) \tag{1.4}$$

where $F(x_j - x_k, T(x_j))$ describes the force exerted from x_k on x_j. Here, $T(x_j)$ denotes a tensor field at location x_j which is given by $T(x) := \chi s(x) \otimes s(x) + l(x) \otimes l(x)$ for orthonormal vector fields $s = s(x)$ and $l = l(x)$ and $\chi \in [0,1]$.

As in the standard particle model (1.2) we assume that the force $F(x_j - x_k, T(x_j))$ is the sum of repulsion and attraction forces. In (1.2), attraction and repulsion forces are aligned along the distance vector $x_j - x_k$ so that the total force $F(x_j - x_k)$ is also aligned along $x_j - x_k$. In the generalised model (1.4), however, the orientation of $F(x_j - x_k, T(x_j))$ depends not only on the distance vector $x_j - x_k$ but additionally on the tensor field $T(x_j)$ at location x_j. More precisely, the attraction force will be assumed to be aligned along the vector $T(x_j)(x_j - x_k)$. Since T depends on a parameter $\chi \in [0, 1]$ the resulting force direction is regulated by χ. In particular, alignment along the distance vector $x_j - x_k$ is included in (1.4) for $\chi = 1$. The additional dependence of (1.4) on the tensor field T introduces an anisotropy to the equation. This anisotropy leads to more complex, anisotropic patterns that do not occur in the simplified model (1.2).

The force F is non-conservative in general so that it cannot be derived from a potential. However, most of the analysis of the interaction models in the literature relies on the existence of an interaction potential as outlined above. A particle interaction model of the form (1.4) with a non-conservative force term that depends on an underlying tensor field T appears not to have been investigated mathematically in the literature yet.

Due to the generality of the formulation of the anisotropic interaction model (1.4) a better understanding of the pattern formation in (1.4) can be regarded as a first step towards understanding anisotropic pattern formation in nature. An example of an N particle model of the form (1.4) is the model introduced by Kücken and Champod in [49], describing the formation of fingerprint patterns based on the interaction of Merkel cells and mechanical stress in the epidermis [46]. Clearly, fingerprint patterns are of great importance in forensic science. Besides, they are increasingly used in biometric applications. Hence, understanding the model, proposed in [49], and in particular its pattern formation result in a better understanding of the fingerprint pattern formation process. This could be used to model fingerprint patterns with certain features in the future. We will investigate this further in [38].

The goal of this work is to study the equilibria of the microscopic model (1.4) and the associated macroscopic model. By considering the large-time limit we investigate the dependence of the model parameters on the resulting transient and steady patterns numerically. In particular, the transition of the equilibrium from ring patterns for $\chi = 1$ to ellipse patterns and finally to stripe patterns for decreasing values of χ is discussed.

Note that the modelling involves multiple scales which can be seen in several different ways. Given the particle model in (1.4) we consider the associated particle density to derive the mean-field limit. Here, the interaction force exhibits short-range repulsion and long-range attraction. The direction of the attraction force depends on the parameter χ which is responsible for different transient and steady state patterns. More precisely, ring equilibria obtained for $\chi = 1$ evolve into ellipse patterns and stripe patterns as χ decreases. Besides, large-time asymptotics are considered for determining the equilibria.

This work is organized as follows. In section 2, a general formulation of an anisotropic N particle model, the specific Kücken-Champod model [49] and the associated mean-field PDE are introduced. The impact of the force alignment and the tensor field as well as the existence of equilibria is discussed in section 3. Section 4 contains a description of the numerical methods used for the microscopic and the mean-field equations. The numerical results include an investigation of the equilibria as well as a comparison with the analytic results.

2. Description of the model

Kücken and Champod introduced a particle model in [49] modelling the formation of fingerprint patterns by describing the interaction between so-called Merkel cells on a domain $\Omega \subseteq \mathbb{R}^2$. Merkel cells are epidermal cells that appear in the volar skin at about the 7th week of pregnancy. From that time onward they start to multiply and organise themselves in lines exactly where the primary ridges arise. The model introduced in [49] models this pattern formation process as the rearrangement of Merkel cells from a random initial configuration into roughly parallel ridges along the lines of smallest compressive stress.

In this section, we describe a general formulation of the anisotropic microscopic model, relate it to the Kücken-Champod particle model and formulate the corresponding mean-field PDE.

2.1. General formulation of the microscopic model. In the sequel we consider N particles at positions $x_j = x_j(t) \in \mathbb{R}^2$, $j = 1, \dots, N$, at time t. The evolution of the particles can be described by (1.4) with initial data $x_j(0) = x_j^{in}$, $j = 1, \dots, N$. Here, $F(x_j - x_k, T(x_j))$ denotes the total force that particle k exerts on particle j subject to an underlying stress tensor field $T(x_j)$ at x_j, describing the local stress field. The dependence on $T(x_j)$ is based on the experimental results in [47] where an alignment of the particles along the local stress lines is observed, i.e. the evolution of particle j at location x_j depends on the the local stress tensor field $T(x_j)$. Note that (1.4) results from Newton's second law by neglecting the inertia term.

The total force F in (1.4) is given by

$$F(d(x_j, x_k), T(x_j)) = F_A(d(x_j, x_k), T(x_j)) + F_R(d(x_j, x_k)) \tag{2.1}$$

for the distance vector $d(x_j, x_k) = x_j - x_k \in \mathbb{R}^2$. Here, F_R denotes the repulsion force that particle k exerts on particle j and F_A is the attraction force exerted on particle j by particle k.

The tensor field $T(x_j)$ at x_j encodes the direction of the fingerprint lines at x_j and is given by $T(x_j) = \chi s(x_j) \otimes s(x_j) + l(x_j) \otimes l(x_j)$ with $\chi \in [0, 1]$. Here, $s = s(x_j) \in \mathbb{R}^2$ and $l = l(x_j) \in \mathbb{R}^2$ are orthonormal vectors, describing the directions of smallest and largest stress, respectively. The repulsion and attraction forces are of the form

$$F_R(d) = f_R(|d|)d \tag{2.2}$$

and

$$F_A(d = d(x_j, x_k), T(x_j)) = f_A(|d|)T(x_j)d, \tag{2.3}$$

respectively, where, again, $d = d(x_j, x_k) = x_j - x_k \in \mathbb{R}^2$.

Remark 2.1. The parameter $\chi \in [0, 1]$ determines the direction of the interaction. For $\chi = 1$ the attraction force between two particles is aligned along their distance vector, while for $\chi = 0$ the attraction between two particles is oriented exactly along the lines of largest stress.

Depending on the choice of the coefficient functions f_R and f_A in (2.2) and (2.3), respectively, the forces are repulsive or attractive according to the following local definition:

Definition 2.2 (Strictly repulsive (attractive) forces) Let the vector field $G = G(x, y)$ be a continuous interaction force, i.e. the vector $G(x, y)$ is the force which is exerted on x by y. Then G at x in direction $x - y$ is strictly repulsive (attractive) if

$$G(x, y) \cdot (x - y) > 0 \qquad (< 0).$$

Remark 2.3. The meaning of this definition is the following. Let y be fixed and let $X = X(t)$ be the trajectory given by

$$\begin{aligned} \frac{\mathrm{d}X}{\mathrm{d}t} &= G(X, y), \\ X(0) &= x \end{aligned}$$

then $|X(t) - y|$ is locally at $t = 0$ strictly monotonically increasing (decreasing).

To justify that F_R and F_A are repulsion and attractive forces, we make assumptions on the coefficient functions f_R and f_A in (2.2) and (2.3), respectively. Besides, assumptions on the total force F in (2.1) are necessary to derive the mean-field PDE. In the sequel, we assume that the following conditions are satisfied:

Assumption 2.4. We assume that $f_R \colon \mathbb{R}^2 \to \mathbb{R}$ and $f_A \colon \mathbb{R}^2 \to \mathbb{R}$ denote smooth, integrable coefficient functions satisfying

$$f_R(|d|) \geqslant 0 \quad \text{and} \quad f_A(|d|) \leqslant 0 \quad \text{for all} \quad d \in \mathbb{R}^2 \tag{2.4}$$

such that the total interaction force F in (2.1) exhibits short-range repulsion and long-range attraction forces along l, i.e. there exists a $d_a > 0$ such that

$$(f_A + f_R)(|d|) \leqslant 0 \quad \text{for} \quad |d| > d_a \qquad \text{and} \qquad (f_A + f_R)(|d|) > 0 \quad \text{for} \quad 0 < |d| < d_a.$$

Also, $F \in C^1$ has bounded total derivatives of order 1, i.e. there exists some $L \geqslant 0$ such that

$$\sup_{x,x' \in \mathbb{R}^2} |D_x F(d(x,x'), T(x))| \leqslant L \quad \text{and} \quad \sup_{x,x' \in \mathbb{R}^2} |D_{x'} F(d(x,x'), T(x))| \leqslant L,$$

where D_x denotes the total derivative with respect to x. This implies that F is Lipschitz continuous in both arguments. In particular, F grows at most linearly at infinitely.

Remark 2.5 (Repulsion and attraction forces). The condition on the coefficient functions f_R and f_A in (2.4) is consistent with Definition 2.2. Besides, it immediately follows from (2.2) and (2.3) that $F(d(x,x'), T(x))$ with $d(x,x') = x - x'$, defined in (2.1), has the following properties:

(1) $F(d(x,x'), T(x)) = -F(-d(x,x'), T(x))$ for all $x, x' \in \mathbb{R}^2$
(2) $F(0, T(x)) = 0$ for all $x \in \mathbb{R}^2$

Remark 2.6 (Conservation of center of mass). It is easy to see from the particle model (1.4) that the center of mass $x_c = \frac{1}{N}\sum_{j=1}^N x_j(0) = \frac{1}{N}\sum_{j=1}^N x_j(t)$ is conserved in time for spatially homogeneous tensor fields T.

Remark 2.7 (Forces for spatially homogeneous tensor fields). If the orthonormal vectors s and l are fixed, the tensor field $T = \chi s \otimes s + l \otimes l$ is spatially homogeneous. In this case the total force defined in (2.1) can be rewritten as

$$F(d,T) = f_A(|d|)\,(\chi(s \cdot d)s + (l \cdot d)l) + f_R(|d|)d.$$

In particular, the total force $F(d,T)$ is aligned along d for $\chi = 1$.

2.2. Kücken-Champod particle model. In the Kücken-Champod particle model [49] a spatially homogeneous tensor field T producing straight parallel ridges, e.g.

$$T = \begin{pmatrix} 1 & 0 \\ 0 & \chi \end{pmatrix},$$

is considered for studying the pattern formation. For more realistic patterns the tensor field is generated from 3D finite element simulations [50, 51] or from images of real fingerprints. The coefficient function f_R of the repulsion force F_R (2.2) in the Kücken-Champod model (1.4) is given by

$$f_R(d) = (\alpha|d|^2 + \beta)\exp(-e_R|d|) \tag{2.5}$$

for $d \in \mathbb{R}^2$ and nonnegative parameters α, β and e_R. The coefficient function f_A of the attraction force (2.3) is given by

$$f_A(d) = -\gamma|d|\exp(-e_A|d|) \tag{2.6}$$

for $d \in \mathbb{R}^2$ and nonnegative constants γ and e_A. For the case that the total force (2.1) exhibits short-range repulsion and long-range attraction along l, we choose the parameters as follows:

$$\alpha = 270, \quad \beta = 0.1, \quad \gamma = 35, \quad e_A = 95, \quad e_R = 100, \quad \chi \in [0,1]. \tag{2.7}$$

The coefficient functions (2.5) and (2.6) for the repulsion and attraction forces (2.2) and (2.3) in the Kücken-Champod model (1.4) are plotted in Figure 1a for the parameters in (2.7) and one can easily check that they satisfy Assumption 2.4. If not stated otherwise, we consider the parameter values in (2.7) for the coefficients (2.5) and (2.6) of the repulsion and attraction forces in the Kücken-Champod model (1.4). The sums of the coefficients of the forces $f_R + f_A$ and $f_R + \chi f_A$ for $\chi = 0.2$ are illustrated in Figure 1b. Note that $f_R + f_A$ and $f_R + \chi f_A$ are the force coefficients along the lines of largest and smallest stress, respectively. For the choice of parameters in (2.7) repulsion dominates for short distances along the lines of largest stress to prevent the collision of particles. Besides, the total force exhibits long-range attraction along the lines of largest stress whose absolute value decreases with the distance between particles. Along the lines of smallest

stress the particles are always repulsive for $\chi = 0.2$, independent of the distance, though the repulsion force gets weaker for longer distances.

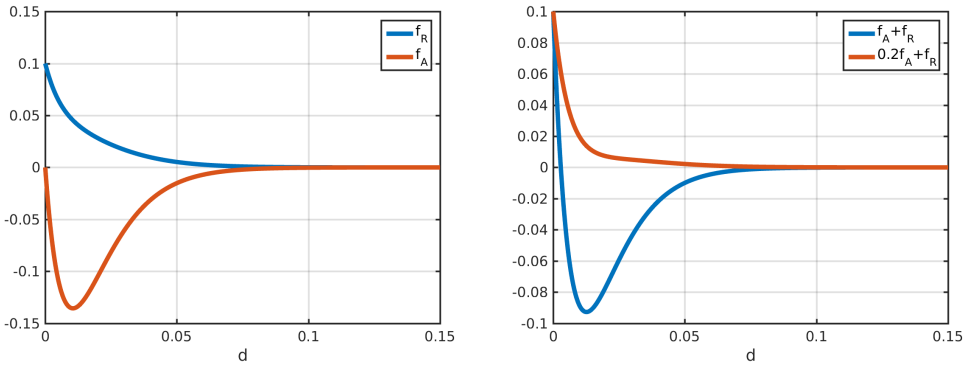

(A) Force coefficients f_R and f_A (B) Total force coefficients

FIGURE 1. Coefficients f_R in (2.5) and f_A in (2.6) of repulsion force (2.2) and attraction force (2.3), respectively, as well as total force coefficients along the lines of largest and smallest stress for $\chi = 0.2$ (i.e. $f_A + f_R$ and $0.2f_A + f_R$, respectively) for parameter values in (2.7)

Remark 2.8 (Existence of an interaction potential). The repulsion force F_R can be derived from a potential, i.e. $F_R = -\nabla W_R$ with

$$W_R(r) = \frac{1}{e_R^4} \exp\left(-e_R|r|\right)\left(\alpha\left(e_R^3|r|^3 + 3e_R^2|r|^2 + 6e_R|r| + 6\right) + \beta e_R^2\left(e_R|r| + 1\right)\right).$$

The attraction force is conservative for $\chi = 1$ only. Then we have $F_A = -\nabla W_A$ with

$$W_A(r) = -\frac{\gamma}{e_A^3} \exp\left(-e_A|r|\right)\left(e_A^2|r|^2 + 2e_A|r| + 2\right),$$

while there exists no potential W_A with $F_A = -\nabla W_A$ for $\chi \in [0, 1)$. Hence, there exists an interaction potential $W = W_A + W_R$ for $\chi = 1$ only.

2.3. Mean-field model. The associated mean-field model for the distribution function $\rho = \rho(t, x)$ at position $x \in \mathbb{R}^2$ and time $t \geqslant 0$ can be derived rigorously in the 1-Wasserstein metric from the microscopic model (1.4) following the procedure described in [45]. The Cauchy problem for the mean-field PDE reads

$$\partial_t \rho(t, x) + \nabla_x \cdot \left[\rho(t, x)\left(F\left(\cdot, T(x)\right) * \rho(t, \cdot)\right)(x)\right] = 0 \qquad \text{in } \mathbb{R}^2 \times \mathbb{R}_+ \tag{2.8}$$

with initial condition $\rho|_{t=0} = \rho^{in}$ in $\mathbb{R}^2$.

Remark 2.9. Given initial data $\rho^{in} \in \mathcal{P}(\mathbb{R}^2)$ where $\mathcal{P}(\mathbb{R}^2)$ denotes the set of Borel probability measures on $\mathbb{R}^2$ then the unique weak solution ρ to the mean-field PDE (2.8) is in $C(\mathbb{R}_+; \mathcal{P}(\mathbb{R}^2))$.

Remark 2.10 (Mean-field limit). Given $X_N = (x_1, \dots, x_N)$, let $\rho_{X_N} = \frac{1}{N}\sum_{j=1}^N \delta_{x_j}$ denote the associated empirical measure on $\mathbb{R}^2$. Further, let $t \to T_t X_N^{in} = (x_1(t), \dots, x_N(t))$ denote the solution of the microscopic model (1.4) with initial data $X_N^{in} = (x_1^{in}, \dots, x_N^{in}) \in (\mathbb{R}^2)^N$. Then, the empirical measure $\rho(t, \mathrm{d}x) = \rho_{T_t X_N^{in}}$ is the weak solution to the mean-field PDE (2.8) with initial condition $\rho|_{t=0} = \rho_{X_N^{in}}$ in $\mathbb{R}^2$.

Let λ denote the Lebesgue measure on $\mathbb{R}^2$ and let $W_1(\mu, \nu)$ be the 1-Wasserstein metric between μ and ν. Let ρ^{in} denote a probability density on $\mathbb{R}^2$ with finite moment of order 1 and for each $N \geqslant 1$ let $X_N^{in} = \left(x_1^{in}, \dots, x_N^{in}\right) \in (\mathbb{R}^2)^N$ be such that the empirical measure $\rho_{X_N^{in}}$ satisfies

$$W_1\left(\rho_{X_N^{in}}, \rho^{in}\right) \to 0 \quad \text{as } N \to \infty.$$

Then,

$$\rho_{T_t X_N^{in}} \rightharpoonup \rho(t,\cdot)\lambda \quad \text{as } N \to \infty$$

in the weak topology of probability measures with convergence rate

$$W_1\left(\mu_{T_t X_N^{in}}, \rho(t,\cdot)\lambda\right) \leqslant e^{2L|t|} W_1\left(\rho_{X_N^{in}}, \rho^{in}\right) \to 0$$

as $N \to \infty$ for each $t \geqslant 0$.

Remark 2.11. For $\chi = 1$, the tensor field T reduces to $T(x) = I_2$ where I_2 denotes the two-dimensional unit matrix. In this case, $F(d, T(x)) = [f_A(d) + f_R(d)]d$ and hence an interaction potential W with $F(d(x,x'), T(x)) = -\nabla_d W(d(x,x'), T(x))$ exists for the Kücken-Champod particle model by Remark 2.8. The mean-field PDE (2.8) is formally the gradient flow of the interaction energy $\mathcal{W}[\rho] = \frac{1}{2}\int_{\mathbb{R}^2} (W(\cdot, T(x)) * \rho)(x)\rho(\mathrm{d}x)$ with respect to the 2-Wasserstein metric.

3. Analysis of the model

In this section, we analyse the particle model (1.4) and the associated mean-field PDE (2.8) where the total force is given by (2.1) and we consider the repulsion force and attraction force in their general form in (2.2) and (2.3), respectively. Besides, we assume that all parameters are constants.

3.1. Interpretation of the total force. In this subsection, we discuss the action of the total force F, defined in (2.1). Note that the parameter $\chi \in [0,1]$ in the definition of the attraction force (2.3) is responsible for the force alignment and thus, the resulting patterns strongly depend on the choice of χ.

Let us firstly consider the gradient flow case $\chi = 1$. As stated in Remark 2.8 the total force in the microscopic model (1.4) can be derived from a potential for the case $\chi = 1$. Thus, the particle model (1.4) and the mean-field PDE (2.8) can be reduced to the corresponding isotropic interaction equations (1.2) and (1.3) which have already been studied extensively in literature. In particular, the solution to (2.8) is radially symmetric for $\chi = 1$ if a radially symmetric initial data is given [10].

Based on the knowledge of the gradient flow case $\chi = 1$ we discuss the influence of the parameter χ by rewriting the total force as the sum of conservative and non-conservative forces. Since the repulsion force (2.2) can be derived from a potential, it is sufficient to rewrite the attraction force (2.3). Note that the attraction force F_A in (2.3) can be rewritten as $F_A = F_{A,1} + F_{A,2}$ where

$$F_{A,1}(d) = f_A(|d|)d$$

and

$$F_{A,2}(d(x_j,x_k), T(x_j)) = f_A(|d|)(T(x_j) - I)d = f_A(|d|)\,(\chi - 1)\,(s(x_j)\cdot d)\,s(x_j),$$

for $d = d(x_j,x_k) = x_j - x_k$, i.e. $F_{A,1}$ is equal to the attraction force for $\chi = 1$ and only depends on the distance vector d, while $F_{A,2}$ is a force in the direction $s(x_j)$. Further note that $F_{A,2}$ vanishes for $\chi = 1$, while there exists an additional force along $s = s(x_j)$ for $\chi \neq 1$. Hence, given a radially symmetric initial distribution, the solution to the mean-field PDE (2.8) is radially symmetric for $\chi = 1$, while the additional force $F_{A,2}$ along s for $\chi \neq 1$ leads to an additional advection along s. Since the coefficient $f_A(|d|)(\chi - 1)$ of $F_{A,2}$ is nonnegative, the additional force along s is repulsive. In particular, we have an additional repulsive force along the vertical axis for the spatially homogeneous stress tensor field T with $s = (0,1)$ and $l = (1,0)$, resulting in an asymmetric solution with respect to the two coordinate axes.

To explain the pattern formation in the Kücken-Champod model (1.4) with coefficient functions (2.5) and (2.6), respectively, one can consider the forces along the lines of largest and smallest stress for different values of χ as illustrated in Figure 2. Note that the total force along the lines of largest stress is independent of χ. For $\chi \in \{0.3, 0.4, \dots, 1\}$, i.e. for $\chi \in [0.3, 1]$ by continuity of the forces, the repulsion forces dominate on short distances, while attraction dominates on long distances along the lines of largest and smallest stress. In particular, the forces along the lines of largest and smallest stress are identical for $\chi = 1$. The equality of the forces along the lines of largest and smallest stress for $\chi = 1$ implies that the solution is radially symmetric if it is initially

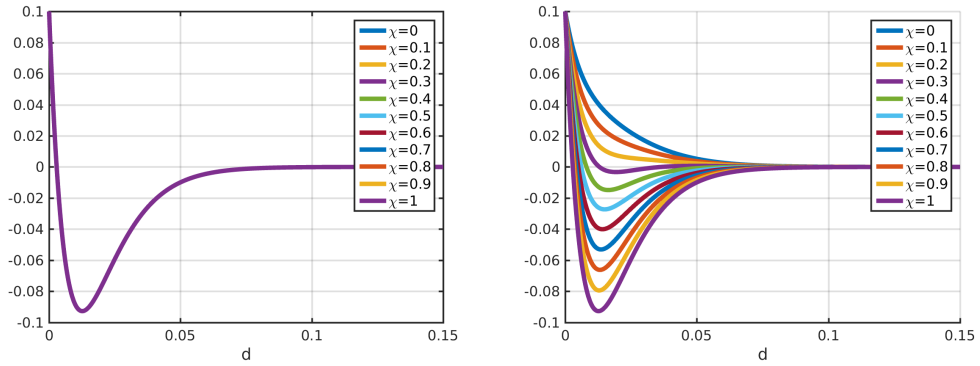

(A) Along lines of largest stress (B) Along lines of smallest stress

FIGURE 2. Total force coefficients along the lines of largest and smallest stress (i.e. $f_A + f_R$ and $\chi f_A + f_R$ for coefficients f_A in (2.6) and f_R in (2.5) of the attraction and the repulsion force for parameter values in (2.7), respectively) for different values of χ

radially symmetric. Note that the smaller χ the larger the area of repulsion along the lines of smallest stress and the more repulsive the total force along the lines of smallest stress. In other words, we have an additional repulsion force along the lines of smallest stress for $\chi < 1$ compared to the force along the lines of largest stress. Due to this additional repulsion force the solution is stretched along the lines of smallest stress for $\chi < 1$. For the spatially homogeneous tensor field $T = \chi s \otimes s + l \otimes l$ with $l = (1, 0)$ and $s = (0, 1)$ the solution is stretched along the vertical axis for $\chi < 1$. The smaller the value of χ, the larger the repulsion force and the more stretching along the vertical axis we have. For $\chi \in \{0, 0.1, 0.2\}$, i.e. for $\chi \in [0, 0.2]$ by continuity of the forces, the total force is purely repulsive as illustrated in Figure 2. Hence, stretching along the entire vertical axis is possible.

3.2. Impact of spatially homogeneous tensor fields. In this section, we discuss that under the assumption that the tensor field is spatially homogeneous it is sufficient to analyse the equilibria of the microscopic and the macroscopic model for the tensor field $T = \chi s \otimes s + l \otimes l$ where $l = (1, 0)$ and $s = (0, 1)$. More precisely, we show that the solution of the particle model (1.4) for any spatially homogeneous tensor field $\tilde{T}$ on $\mathbb{R}^2$ can be interpreted as a coordinate transform of the solution of the particle model (1.4) for the spatially homogeneous tensor field $T = \chi s \otimes s + l \otimes l$ with $l = (1, 0)$ and $s = (0, 1)$. A similar statement can also be shown for the equilibrium to the microscopic model (1.4). For detailed computations see Remark A.1 in Appendix A. To show a similar statement for the mean-field PDE (2.8) we define the concept of an equilibrium state based on Remark 2.9.

Definition 3.1 (Equilibrium state of (2.8)) A probability measure $\mu \in \mathcal{P}(\mathbb{R}^2)$ is said to be an equilibrium state of the mean-field PDE (2.8) if

$$(F(\cdot, T(x)) * \mu)(x) = 0 \qquad \text{for all} \quad x \in \operatorname{supp}(\mu). \tag{3.1}$$

One can show that an equilibrium state of the mean-field equation (2.8) for any spatially homogeneous tensor field $\tilde{T}$ on $\mathbb{R}^2$ is the coordinate transform of an equilibrium state to the mean-field equation (2.8) for the spatially homogeneous tensor field $T = \chi s \otimes s + l \otimes l$ with $l = (1, 0)$ and $s = (0, 1)$. For further details see Remark A.2.

3.3. Existence of equilibria. As defined in Definition 3.1 an equilibrium state of the mean-field PDE (2.8) has to satisfy (3.1). Based on the discussion on the action of the total force in section **3.1** we discuss possible shapes of equilibria of the mean-field PDE (2.8) in this section.

To get a better understanding of the impact of the tensor field on the shapes of the equilibria, we restrict ourselves on spatially homogeneous tensor fields. As outlined in section **3.2** it is sufficient to consider the tensor field $T = \chi s \otimes s + l \otimes l$ with $l = (1,0)$ and $s = (0,1)$ in the sequel. Note that the forces along l are assumed to be repulsive-attractive, while the forces along s depend significantly on the choice of χ and may be repulsive, repulsive-attractive-repulsive or repulsive-attractive. Further note that the forces only depend on the distance vector for spatially homogeneous tensor fields.

To simplify the analysis, we make the following assumption on F in addition to Assumption 2.4 in this section:

Assumption 3.2. We assume that F is strictly decreasing along l on the interval $[0, d_e]$ for some $d_e > d_a$ where d_a is defined in Assumption 2.4. In particular, $f_A + f_R$ is strictly decreasing on $[0, d_e]$.

Remark 3.3. Assumption 3.2 is clearly satisfied for the force coefficients (2.6) and (2.5) in the Kücken-Champod model (1.4) with parameter values in (2.7) if d_e is the maximum of $f_A + f_R$.

3.3.1. *Ellipse pattern.* In this subsection, we consider ellipse patterns and investigate whether they are equilibria to the mean-field PDE (2.8). Since stretching along the vertical axis is expected for the tensor field $T = \chi s \otimes s + l \otimes l$ with $l = (1,0)$ and $s = (0,1)$ by the discussion in section **3.1** we consider an ellipse whose major axis is parallel to the vertical axis. Note that the ellipse pattern can be regarded as a generalisation of the ring pattern.

Definition 3.4 Let $R > 0$ and let $r \geqslant 0$. The ellipse state whose minor and major axis are of lengths R and $R + r$, respectively, is the probability measure which is uniformly distributed on $\{x = (x_1, x_2) \in \mathbb{R}^2 \colon x_1 = R\cos\phi,\ x_2 = (R + r)\sin\phi\}$. We denote this probability measure by $\delta_{(R,r)}$.

Remark 3.5. It is sufficient to restrict ourselves to probability measures with center of mass $(0,0)$ because of the spatial homogeneity of the tensor field.

First, we restrict ourselves to non=trivial ring states $\delta_{(R,0)}$ of radius $R > 0$, i.e. we consider the special case of ellipse states where $r = 0$.

Remark 3.6 (Existence of ring equilibria). The existence of ring equilibria for repulsive-attractive potentials that do not decay faster than $1/d^2$ as $d \to \infty$ has already been discussed in [4]. However, the force coefficients (2.5) and (2.6) in the Kücken-Champod model [49] decay exponentially fast as $d \to \infty$. Besides, a repulsive-attractive potential only exists for $\chi = 1$.

To analyse the ring equilibria we distinguish between the two cases $\chi = 1$ and $\chi \in [0,1)$, starting with the case $\chi = 1$.

Lemma 3.7 *Let $\chi = 1$. The probability measure $\delta_{(R,0)}$ is a non-trivial ring equilibrium to (2.8) for radius $R > 0$ if and only if*

$$\int_0^\pi (f_A + f_R)\left(R\sqrt{(1-\cos\phi)^2 + \sin^2\phi}\right)(1-\cos\phi)\,\mathrm{d}\phi = 0. \tag{3.2}$$

Proof. Note that for $\chi = 1$ the total force F is aligned along distance vector d by Remark 2.7. By Definition 3.1 and by symmetry it suffices to show for $\chi = 1$ that there exists $R > 0$ such that

$$(F(\cdot,T) * \delta_{(R,0)})((R,0)) = \int_{\partial B(0,R)} F((R,0) - x, T)\,\mathrm{d}s = \int_0^{2\pi} F(R(1-\cos\phi, -\sin\phi), T) R\,\mathrm{d}\phi = 0$$

for non-trivial ring equilibria. A change of variables yields

$$\int_\pi^{2\pi} F(R(1-\cos\phi, -\sin\phi), T) R\,\mathrm{d}\phi = \int_0^\pi F(R(1-\cos\phi, \sin\phi), T) R\,\mathrm{d}\phi.$$

Hence, by using the simplified form of $F(d,T) = (f_A + f_R)(|d|)d$ for $\chi = 1$ this implies that it is sufficient to show the existence of $R > 0$ such that

$$R^2 \int_0^\pi (f_A + f_R)\left(R\sqrt{(1-\cos\phi)^2 + \sin^2\phi}\right)(1-\cos\phi)\,\mathrm{d}\phi = 0.$$

Since we are interested in non-trivial ring equilibria with radius $R > 0$ the condition finally reduces to (3.2). □

Proposition 3.8 *Let $\chi = 1$. There exists at most one radius $R \in (0, \frac{d_e}{2}]$ such that the ring state $\delta_{(R,0)}$ of radius R is a non-trivial equilibrium to the mean-field PDE (2.8). If*

$$\int_0^\pi (f_A + f_R)\left(\frac{d_e}{2}\sqrt{(1-\cos\phi)^2 + \sin^2\phi}\right)(1-\cos\phi)\,\mathrm{d}\phi < 0 \tag{3.3}$$

there exists a unique $R \in (\frac{d_a}{2}, \frac{d_e}{2}]$ such that the ring state $\delta_{(R,0)}$ of radius R is a non-trivial equilibrium.

Proof. Consider the left-hand side of (3.2) as a function of R denoted by $G(R)$. By deriving $G(R)$ with respect to R and using Assumption 3.2, one can easily see that $G(R)$ is strictly decreasing as a function of R on $[0, \frac{d_e}{2}]$. Note that $G(0) > 0$, $G(R) > 0$ for $R \leqslant \frac{d_a}{2}$ and f_A, f_R are continuous by Assumption 2.4 on the total force. This concludes the proof. □

Remark 3.9. One can easily check that (3.3) is satisfied for the force coefficients (2.5) and (2.6) in the Kücken-Champod model (1.4) with parameter values in (2.7) if d_e is the maximum of $f_A + f_R$. In particular, this implies that there exists a unique non-trivial ring equilibrium of radius $R \in (\frac{d_a}{2}, \frac{d_e}{2}]$ to (2.8) for the forces in the Kücken-Champod model for $\chi = 1$.

The case $\chi \in [0, 1)$ can be analysed similarly as the one for $\chi = 1$ for ring patterns except that some of the symmetry arguments do not hold.

Proposition 3.10 *Let $\chi \in [0, 1)$. There exists no $R \in (0, \frac{d_e}{2}]$ such that the ring state $\delta_{(R,0)}$ is an equilibrium to the mean-field PDE (2.8).*

Proof. For $\chi = 1$, $(F(\cdot, T) * \delta_{(R,0)})((R, 0)) = 0$ is equivalent to (3.2) by Lemma 3.7, based on the property $(F(\cdot, T) * \delta_{(R,0)})((R, 0)) \cdot s = 0$. Since $F(d, T) = f_A(|d|)(d_1, \chi d_2) + f_R(|d|)d$ where $d = (d_1, d_2)$, (3.2) also has to be satisfied for $\chi \in [0, 1)$. Similarly as in the proof of Lemma 3.7 one can show that

$$(F(\cdot, T) * \delta_{(R,0)})((0, R)) = \int_0^{2\pi} F(R(-\cos\phi, 1-\sin\phi), T) R\,\mathrm{d}\phi = 0$$

is equivalent to

$$\int_{\pi/2}^{3\pi/2} (\chi f_A + f_R)\left(R\sqrt{\cos^2\phi + (1-\sin\phi)^2}\right)(1-\sin\phi)\,\mathrm{d}\phi = 0 \tag{3.4}$$

for $R > 0$. Note that (3.2) is equivalent to (3.4) for $\chi = 1$ by symmetry so that the equilibrium of radius $R \in (0, \frac{d_e}{2}]$ from Proposition 3.8 satisfies (3.2) and (3.4) simultaneously for $\chi = 1$. However, (3.2) and (3.4) are not satisfied simultaneously for any $R \in (0, \frac{d_2}{2}]$ and any $\chi \in [0, 1)$ which concludes the proof. □

Since the ellipse state $\delta_{(R,r)}$ where $R, r \geqslant 0$ can be regarded as a generalization of the ring state the ellipse pattern can be analysed in a similar way, resulting in the following corollary.

Corollary 3.11 *Let $\chi \in [0, 1]$ be given. Let $R \in (0, \frac{d_e}{2})$ and let $r_e > 0$ such that*

$$\sqrt{R^2(1-\cos\phi)^2 + (R+r)^2\sin^2\phi} \leqslant d_e \quad \text{for all} \quad \phi \in [0, \pi],\ r \in [0, r_e] \tag{3.5}$$

is satisfied. Then, there exists at most one $r \in [0, r_e)$ such that the ellipse $\delta_{(R,r)}$ is an equilibrium to the mean-field PDE (2.8).

Proof. Similarly as in the proof of Lemma 3.7 one can show that necessary conditions for non-trivial ellipse equilibria to (2.8) for $\chi \in [0, 1]$ satisfy

$$\int_0^\pi (f_A + f_R)\left(\sqrt{R^2(1-\cos\phi)^2 + (R+r)^2\sin^2\phi}\right)(1-\cos\phi)\,\mathrm{d}\phi = 0 \tag{3.6}$$

and

$$\int_{\pi/2}^{3\pi/2} (\chi f_A + f_R)\left(\sqrt{R^2\cos^2\phi + (R+r)^2(1-\sin\phi)^2}\right)(1-\sin\phi)\,\mathrm{d}\phi = 0. \tag{3.7}$$

Note that for $R \in (0, \frac{d_e}{2})$ there exists $r_e > 0$ such that (3.5) is satisfied. Let $R \in (0, \frac{d_e}{2})$ be given and let $r_e > 0$ be chosen accordingly. The derivative of the left-hand side of (3.6) with respect to r is negative on $[0, r_e)$, implying that the left-hand side of (3.6) is strictly decreasing in r for $R \in (0, \frac{d_e}{2})$ given. □

Remark 3.12 (Choice of parameters (R, r) in the ellipse pattern). Let $\bar{R}$ denote the radius of the unique ring equilibrium from Proposition 3.8. Then the tuple $(\bar{R}, 0)$ satisfies (3.6) and (3.7) for $\chi = 1$. Since one can show as in Lemma 3.11 that the left-hand side of (3.6) is strictly decreasing in R on $[0, \frac{d_e}{2})$ for $r > 0$ sufficiently small, this implies that all possible tuples satisfying condition (3.6) can be determined from $(\bar{R}, 0)$ by increasing r and decreasing R. In other words, this means that the shorter the minor axis of the ellipse, the longer the major axis. Hence, using condition (3.6) one can determine all possible tuples (R, r) for ellipse patterns independently of χ.

Remark 3.13 (Dependence of ellipse pattern on χ). Note that the left-hand side of (3.7) is decreasing in χ by Assumption 2.4. Further note that for χ sufficiently close to 1, Assumption 3.2 is satisfied for $\chi f_A + f_R$ and the left-hand side of (3.7) thus decreases as a function of R and as a function of r, respectively. Since (3.7) is satisfied for $(\bar{R}, 0)$ and $\chi = 1$, this implies that for χ decreasing from 1 the values of R and r have to be adapted accordingly to satisfy (3.7), i.e. if χ decreases it is necessary that R decreases and r increases as $r \geqslant 0$ to fulfil (3.7). In particular, this means that for every $\chi \in [0, 1]$ such that $\chi f_A + f_R$ satisfies Assumption 3.2 there exists at most one tuple (R, r) such that the corresponding ellipse pattern $\delta_{(R,r)}$ is an equilibrium. The smaller the value of χ the longer the major and the shorter the minor axis of the possible ellipse equilibrium, i.e. the smaller the value of χ the more the ellipse is stretched along the vertical axis.

3.3.2. *Stripe pattern.* Based on the discussion in section **3.1** for the tensor field $T = \chi s \otimes s + l \otimes l$ with $l = (1, 0)$ and $s = (0, 1)$, we consider different shapes of vertical stripe patterns and discuss whether they are equilibria.

Definition 3.14 Let $x_{c,1}$ denote the x_1 coordinate of the center of mass $x_c = (x_{c,1}, x_{c,2}) \in \mathbb{R}$. Then we denote by $\delta_{(x_{c,1},\cdot)}$ the measure which is uniformly distributed on $\{x = (x_1, x_2) \in \mathbb{R}^2 \colon x_1 = x_{c,1}\}$.

Remark 3.15. Note that $\delta_{(x_{c,1},\cdot)}$ is the Lebesgue measure on $\mathbb{R}^2$ restricted to the stripe at $x_1 = x_{c,1}$ and is a locally finite measure, but not a probability measure. However, in terms of modeling one can consider the associated probability measure on the two-dimensional unit torus $\mathbb{T}^2$ instead of the full space $\mathbb{R}^2$.

Proposition 3.16 *Given $x_{c,1} \in \mathbb{R}$, the measure $\delta_{(x_{c,1},\cdot)}$ satisfies condition (3.1) for equilibria of the mean-field PDE (2.8) for any force satisfying Assumption 2.4 and any $\chi \in [0, 1]$.*

Proof. Condition (3.1) for equilibria is satisfied by force properties 1 and 2 in Remark 2.5. □

Remark 3.17 (Stability). Even though the measure $\delta_{(x_{c,1},\cdot)}$ satrisfies condition (3.1) for equilibria for all $\chi \in [0, 1]$, it is not necessarily a stable solution of the mean-field PDE (2.8). To obtain a stable vertical stripe pattern it is necessary that the forces along the vertical axis s are significantly larger than along l. For repulsive-attractive forces along l and entirely repulsive forces along s, e.g. for the parameter values in (2.7), $\chi \in [0, 0.2]$ and the force coefficients (2.5) and (2.6) in the Kücken-Champod model, the solution to (2.8) is stretched along the whole vertical axis due to the lack of attraction forces along that axis and thus stability is possible.

Other possible solutions to the mean-field PDE (2.8) satisfying condition (3.1) include measures which are uniformly distributed on certain intervals along the vertical axis, i.e. on $\{x = (x_1, x_2) \in \mathbb{R}^2 \colon x_1 = x_{c,1}, x_2 \in [a, b]\}$ for some constants $a < b$, as well as measures which are uniformly distributed on unions of distinct intervals. The former occur if the total force is repulsive-attractive

so that the attraction force restricts the stretching of the solution to certain subsets of the vertical axis. The latter which look like dashed lines parallel to the vertical axis can be realised by repulsive-attractive-repulsive forces, i.e. repulsive-attractive forces may lead to accumulations on subsets of the vertical axis while the additional repulsion force acting on long distances is responsible for the separation of the different subsets.

After considering these one-dimensional patterns, the question arises whether the corresponding two-dimensional vertical stripe pattern of width Δ satisfies the equilibrium condition (3.1) for any $\Delta > 0$.

Remark 3.18. Let $\Delta > 0$ and consider the two-dimensional vertical stripe pattern of width Δ, given by

$$g_\Delta(x) = g_\Delta(x_1, x_2) = \begin{cases} \frac{1}{\Delta} & x_1 \in \left[x_{c,1} - \frac{\Delta}{2}, x_{c,1} + \frac{\Delta}{2}\right] \\ 0 & \text{otherwise} \end{cases}.$$

We assume that g_Δ satisfies the equilibrium condition (3.1) for the mean-field PDE (2.8), i.e. $g_\Delta \, (F * g_\Delta) = 0$, implying

$$\int_{\left[x_{c,1} - \frac{\Delta}{2}, x_{c,1} + \frac{\Delta}{2}\right] \times \mathbb{R}} F(x - x', T) \, \mathrm{d}x' = 0 \quad \text{for all} \quad x \in \left[x_{c,1} - \frac{\Delta}{2}, x_{c,1} + \frac{\Delta}{2}\right] \times \mathbb{R}.$$

By linear transformations this reduces to

$$\int_{\left[-\frac{\Delta}{2}, \frac{\Delta}{2}\right] \times \mathbb{R}} F((x_1, 0) - x', T) \, \mathrm{d}x' = 0 \quad \text{for all} \quad x_1 \in \left[-\frac{\Delta}{2}, \frac{\Delta}{2}\right].$$

Force property 1 in Remark 2.5 implies

$$e_1 \cdot \int_{\left[-\frac{\Delta}{2}, \frac{\Delta}{2}\right] \times \mathbb{R}} F((x_1, 0) - x', T) \, \mathrm{d}x' = 0 \quad \text{for all} \quad x_1 \in \left[-\frac{\Delta}{2}, \frac{\Delta}{2}\right]$$

and again by force property 1 in Remark 2.5 we have

$$e_1 \cdot \int_{[x_1, \Delta - x_1] \times \mathbb{R}} F(x', T) \, \mathrm{d}x' = 0 \quad \text{for all} \quad x_1 \in \left[0, \frac{\Delta}{2}\right). \tag{3.8}$$

Hence the equilibrium state can only occur for special choices of the interaction force F. In general, (3.8) is not satisfied and thus g_Δ is not an equilibrium state of the mean-field PDE.

4. Numerical methods and results

In this section, we investigate the long-time behaviour of solutions to the Kücken-Champod model (1.4) and the corresponding mean-field PDE (2.8) numerically. In particular, we study the pattern formation process numerically.

We consider the domain $\Omega = \mathbb{T}^2$ where $\mathbb{T}^2$ is the 2-dimensional unit torus that can be identified with the unit square $[0, 1) \times [0, 1) \subset \mathbb{R}^2$ with periodic boundary conditions. In fact, the numerical simulations indicate that periodic boundary conditions are a very good choice and have several advantages over other boundary conditions. To guarantee that particles can only interact within a finite range we assume that they cannot interact with each other if they are separated by a distance of at least 0.5 in each spatial direction, i.e. for $i \in \{1, 2\}$ and all $x \in \Omega$ we require that $F(x - x', T(x)) \cdot e_i = 0$ for $|x - x'| \geqslant 0.5$ where e_i denotes the standard basis for the Euclidean plane. This property of the total interaction force F in (2.1) is referred to as the minimum image criterion [41]. Note that the coefficient functions f_R and f_A in (2.5) and (2.6) in the Kücken-Champod model (1.4) satisfy the minimum image criterion if a spherical cutoff radius of length 0.5 is introduced for the repulsion and attraction forces.

Remark 4.1 (Minimum image criterion). The minimum image criterion is a natural condition for large systems of interacting particles on a domain with periodic boundary conditions. In numerical simulations, it is sufficient to record and propagate only the particles in the original simulation box. Besides, the minimum image criterion guarantees that the size of the domain is large enough

compared to the range of the total force. In particular, non-physical artefacts due to periodic boundary conditions are prevented.

4.1. Numerical methods. We discuss the numerical methods for solving the Kücken-Champod model (1.4) and the mean-field PDE (2.8), respectively, for spatially homogeneous tensor fields T.

4.1.1. *Particle simulation.* To solve the N particle ODE system (1.4) we consider periodic boundary conditions and apply either the simple explicit Euler scheme or higher order methods such as the Runge-Kutta-Dormand-Prince method, all resulting in very similar simulation results.

4.1.2. *Mean-field simulation.* Numerical methods for solving the multidimensional aggregation equation (1.3) for a wide range of kernels were developed in [23, 35]. In [23] a positivity preserving entropy decreasing finite volume scheme for non-linear nonlocal equations with a gradient flow structure has been proposed, while in [35] a particle method is introduced in which the kernel is regularized by convolution with a smooth, rapidly decreasing mollifier. However, we are particularly interested in solving the mean-field equation (2.8) with anisotropic interaction forces. We solve the mean-field equation (2.8) with periodic boundary conditions numerically by applying a non-linear version of the one-dimensional upwind scheme in each spatial direction. Given the numerical solution at a certain time, the length of the next time step is chosen as large as possible such that the CFL condition is satisfied. In future work, more advanced numerical methods for solving the macroscopic model (2.8) with anisotropic interaction forces could be developed.

4.2. Numerical results. We show numerical results for the Kücken-Champod model (1.4) and the macroscopic model (2.8) on the domain $\Omega = T^2$ where the force coefficients are given by (2.5) and (2.6). In particular, we investigate the patterns of the corresponding stationary solutions. Unless stated otherwise we consider the parameter values in (2.7) and the spatially homogeneous tensor field $T = \chi s \otimes s + l \otimes l$ with $l = (1, 0)$ and $s = (0, 1)$. Besides, we assume that the initial condition is a Gaussian with mean $\mu = 0.5$ and standard deviation $\sigma = 0.005$ in each spatial direction.

4.2.1. *Comparison of particle and mean-field simulations.* In Figure 3 the stationary solutions of the Kücken-Champod model (1.4) for $N = 1200$ particles and of the mean-field PDE (2.8) for a spatial discretization of 100 grid points in each spatial direction are shown. One can clearly see that the obtained numerical results are consistent with the analysis in section 3. In particular, the stationary solution is stretched along the vertical axis for $\chi = 0.2$ in comparison to the radially symmetric stationary solution for $\chi = 1$.

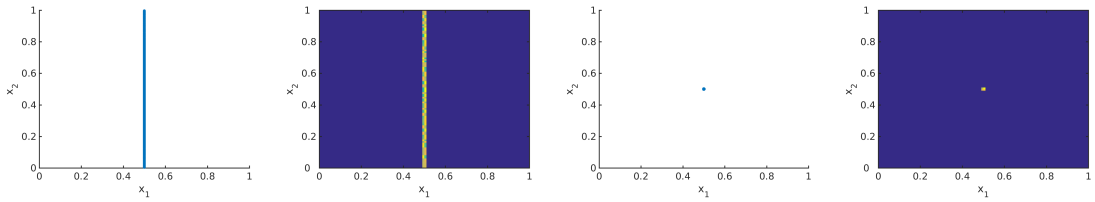

(A) $\chi = 0.2$ (B) $\chi = 1$

FIGURE 3. Stationary solution to the Kücken-Champod model (1.4) (left) and the corresponding mean-field PDE (2.8) (right) for different values of χ

4.2.2. *Boundary conditions.* In [49] where the Kücken-Champod model has firstly been introduced spring forces are considered to force the cells to stay in the computational domain. However, the nature of these spring forces is not given. Since linear or exponential forces at the boundaries result in even more parameters which is not helpful for understanding the qualitative behaviour of solutions to the model, we compare the numerical solutions for periodic and reflecting boundary conditions for the particle model as well as periodic, homogeneous Neumann and homogeneous

Dirichlet boundary conditions for the macroscopic model. The numerical results strongly indicate that periodic boundary conditions are most natural, in particular because one could clearly see that the stationary solution is aligned along the lines of smallest stress, i.e. along the vertical axis for the considered tensor field T, which coincides with the observations in [49]. Furthermore, both homogeneous Dirichlet and homogeneous Neumann boundary conditions result in undesirable artefacts and unnatural clusterings of the stationary solution. Thus, we assume periodic boundary conditions in the sequel.

4.2.3. *Dependence on initial distribution.* The stationary solution to (1.4) for $N = 1200$ particles is shown in Figure 4 for $\chi = 0.2$ and $\chi = 0.7$, respectively, for different initial data. One can clearly see that the long-time behaviour of the solution depends on the chosen initial conditions. The numerical solution underlines that particles remain isolated or build small clusters if they are initially too far apart from the other particles, i.e. if the distances between the particles are so large that the corresponding interaction forces are negligible. Further note that for $\chi = 0.2$ and randomly uniformly distributed initial data the convergence is very slow and very interesting patterns occur at different times t as illustrated in Figure 5. To understand the influence of the underlying tensor field T and the resulting movement of the particles, in the sequel we restrict ourselves to Gaussian initial data with mean $\mu = 0.5$ and standard deviation $\sigma = 0.005$ in each spatial direction so that all particles can initially interact with each other for the given parameter values in (2.7).

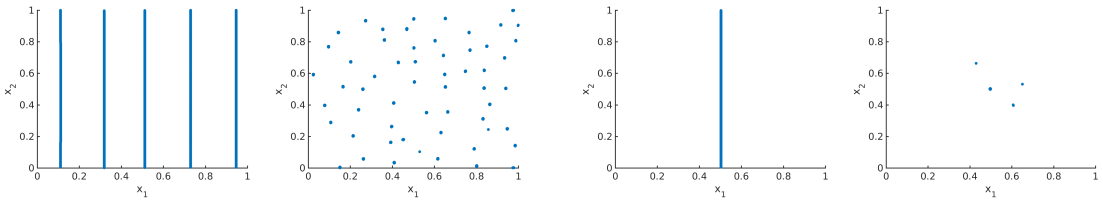

(A) $\chi = 0.2$ (B) $\chi = 0.7$ (C) $\chi = 0.2$ (D) $\chi = 0.7$

Randomly uniformly distributed Gaussian with $\sigma = 0.05$

FIGURE 4. Stationary solution to the Kücken-Champod model (1.4) for different initial data for $\chi = 0.2$ (left) and $\chi = 0.7$ (right)

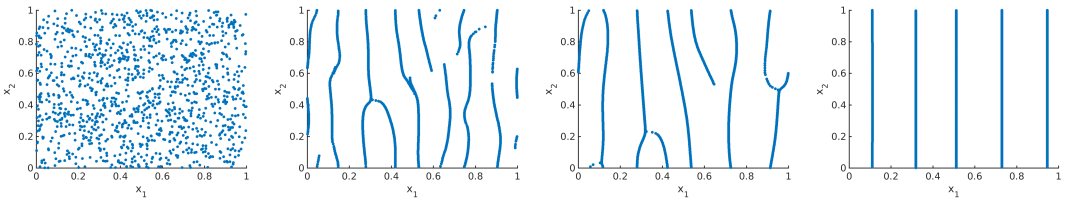

(A) $t = 0$ (B) $t = 50000$ (C) $t = 110000$ (D) $t = 710000$

FIGURE 5. Numerical solution to the Kücken-Champod model (1.4) for randomly uniformly distributed initial data for $\chi = 0.2$ and different times t

4.2.4. *Evolution of the pattern.* In Figure 6, the numerical solution of the particle model (1.4) for $N = 1200$ is shown for $\chi = 0$, $\chi = 0.2$ and $\chi = 1.0$ for different times t. One can clearly see that the solution for $\chi = 0$ and $\chi = 0.2$, respectively, is stretched along the vertical axis, i.e. along $s = (0, 1)$, as time increases. This is consistent with the observations in section **3.1** since

the forces along the vertical axis for $\chi = 0$ and $\chi = 0.2$ are repulsive. Besides, the convergence to the equilibrium state is very fast for $\chi = 1$ compared to $\chi = 0$ and $\chi = 0.2$.

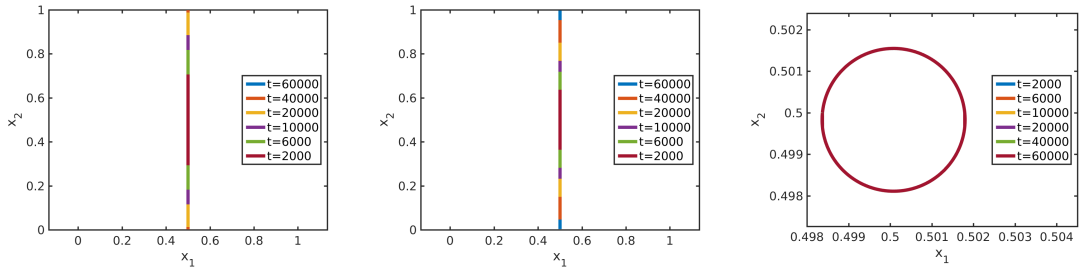

(A) $\chi = 0$ (B) $\chi = 0.2$ (C) $\chi = 1$

FIGURE 6. Numerical solution to the Kücken-Champod model (1.4) for different times t and different values of χ

4.2.5. *Convergence to equilibrium.* In Figure 7 the decay of the distance to equilibrium for the numerical solution to the Kücken-Champod model (1.4) for $N = 1200$ and randomly uniformly distributed initial data is shown in the total variation norm for $\chi = 0.2$ and $\chi = 1$ where linear and semilogarithmic axis are consider in Figures 7a and 7b, respectively. The exponential convergence rates can be estimated by linear regression as $-3.5644 \cdot 10^{-12}$ and $-3.1499 \cdot 10^{-11}$ for $\chi = 0.2$ and $\chi = 1$, respectively. In particular, the convergence for $\chi = 1$ is significantly faster than for $\chi = 0.2$ which is also observed in Figure 6.

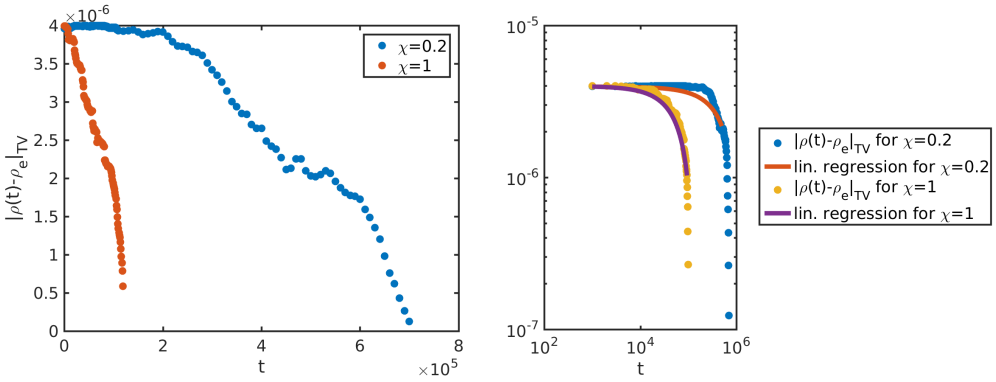

(A) Linear axes (B) Semilogarithmic axes

FIGURE 7. Decay of the distance to equilibrium for the numerical solution to the Kücken-Champod model (1.4) for randomly uniformly distributed initial data and for different values of χ using different scalings

4.2.6. *Dependence on parameter χ.* In this section we investigate the dependence of the equilibria to (1.4) on the parameter χ which strongly influences the pattern formation. The stationary solution to (1.4) for $N = 1200$ is displayed for different values of χ in Figures 8 and 9. In Figure 8 one can see that the size of the pattern is significantly larger for small values of χ due to stretching along the vertical axis (cp. section 3), evolving from a 1D stripe pattern of equally distributed particles along the entire vertical axis via a shorter vertical line to more concentrated patterns.

The patterns for different values of χ are shown in Figure 9 by considering different scalings. As χ increases the equilibrium evolves from a straight line into a standing ellipse and finally into

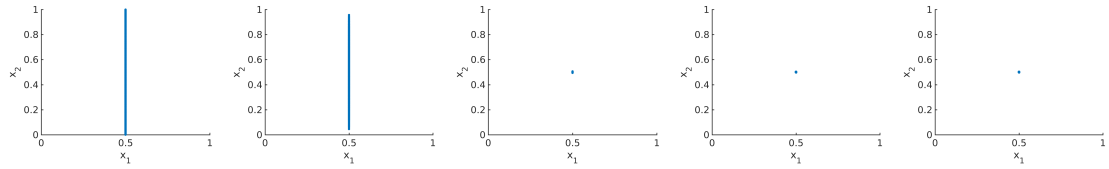

(A) $\chi = 0.08$ (B) $\chi = 0.24$ (C) $\chi = 0.40$ (D) $\chi = 0.56$ (E) $\chi = 0.72$

FIGURE 8. Stationary solution to the Kücken-Champod model (1.4) for different values of χ in terms of size

a ring for $\chi = 1.0$. Note that the length of the minor axis of the ellipse increases as χ increases, while the length of the major axis of the ellipse gets shorter.

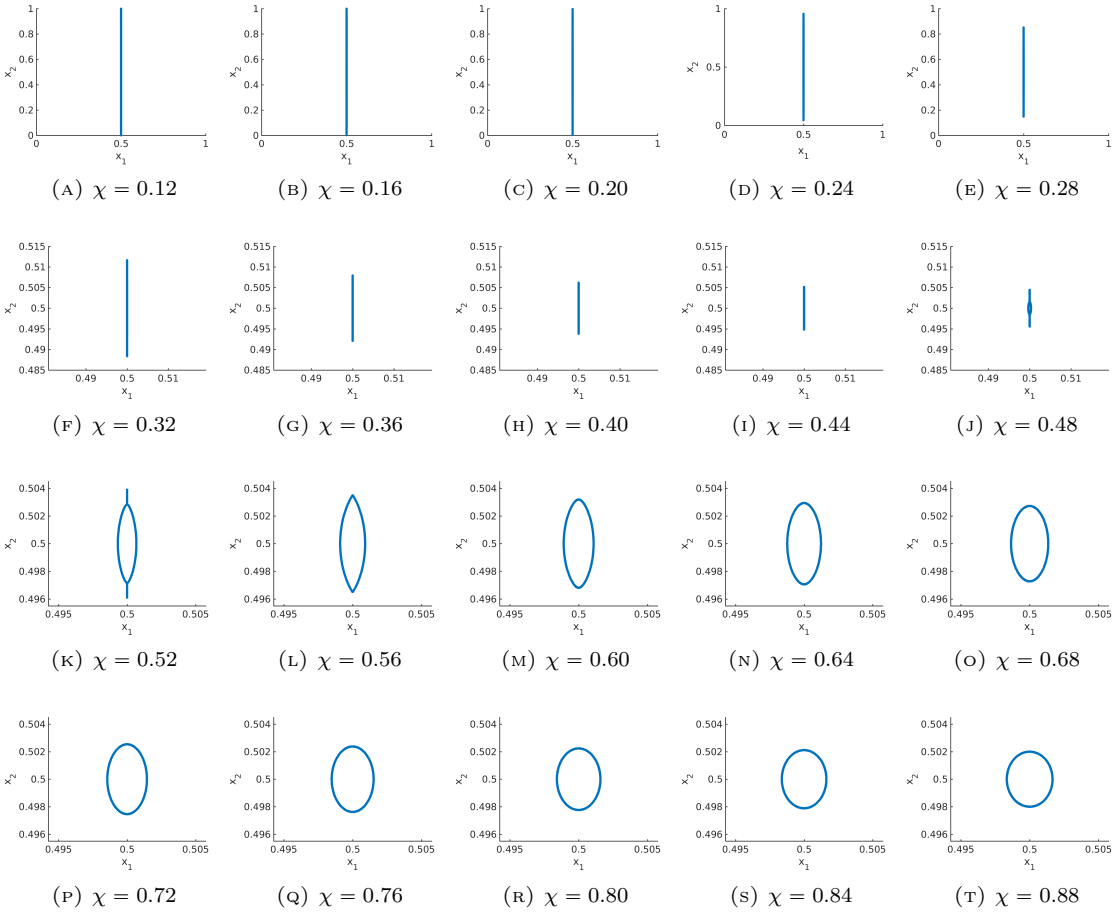

(A) $\chi = 0.12$ (B) $\chi = 0.16$ (C) $\chi = 0.20$ (D) $\chi = 0.24$ (E) $\chi = 0.28$

(F) $\chi = 0.32$ (G) $\chi = 0.36$ (H) $\chi = 0.40$ (I) $\chi = 0.44$ (J) $\chi = 0.48$

(K) $\chi = 0.52$ (L) $\chi = 0.56$ (M) $\chi = 0.60$ (N) $\chi = 0.64$ (O) $\chi = 0.68$

(P) $\chi = 0.72$ (Q) $\chi = 0.76$ (R) $\chi = 0.80$ (S) $\chi = 0.84$ (T) $\chi = 0.88$

FIGURE 9. Stationary solution to the Kücken-Champod model (1.4) for different values of χ in terms of patterns using different axis scalings

4.2.7. *Dependence on parameter e_R.* In Figure 10 the stationary solution to (1.4) for $N = 1200$ and $\chi = 0.2$ is shown for different values of e_R where a ring of radius 0.005 with center $(0.5, 0.5)$ is chosen as initial data. One can clearly see that the size of accumulations increases for e_R increasing due to strong long-range repulsion forces for smaller values of e_R. Besides, the stationary solution is spread over the entire domain for smaller values of e_R. In particular, the solution is spread along the entire horizontal axis. This can be explained by the fact that for smaller values of e_R

the total force along the lines of largest stress, i.e. along the horizontal axis, is no longer short-range repulsive and long-range attractive, but short-range repulsive, medium-range attractive and long-range repulsive and the long-range repulsion is the stronger the smaller the value of e_R.

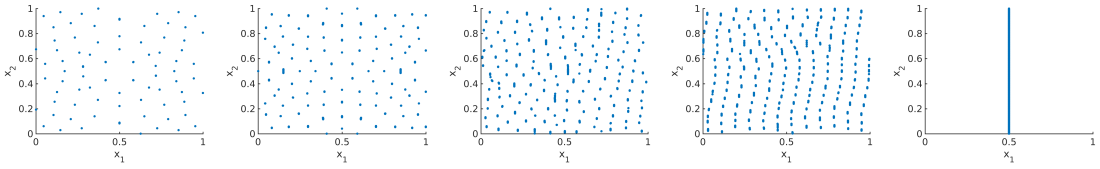

(A) $e_R = 40$ (B) $e_R = 50$ (C) $e_R = 60$ (D) $e_R = 70$ (E) $e_R = 80$

FIGURE 10. Stationary solution to the Kücken-Champod model (1.4) for $\chi = 0.2$ and different values for e_R

4.2.8. *Dependence on the size of the attraction force.* In this section, we assume that the total force is given by $F(d,T) = \delta F_A(d,T) + F_R(d)$ for $\delta \in [0,1]$ for the spatially homogeneous tensor field $T = \chi s \otimes s + l \otimes l$ with $l = (1,0)$ and $s = (0,1)$ instead of (2.1). We investigate the influence of the size of the attraction force F_A on stationary patterns by varying its coefficients. While the force is repulsive for small values of δ, resulting in a stationary solution spread over the entire domain, stripe patterns and ring patterns for $\chi = 0.2$ and $\chi = 1$, respectively, arise as δ increases as shown in Figures 11. Note that the radius of the ring pattern decreases as δ increases due to an increasing attraction force.

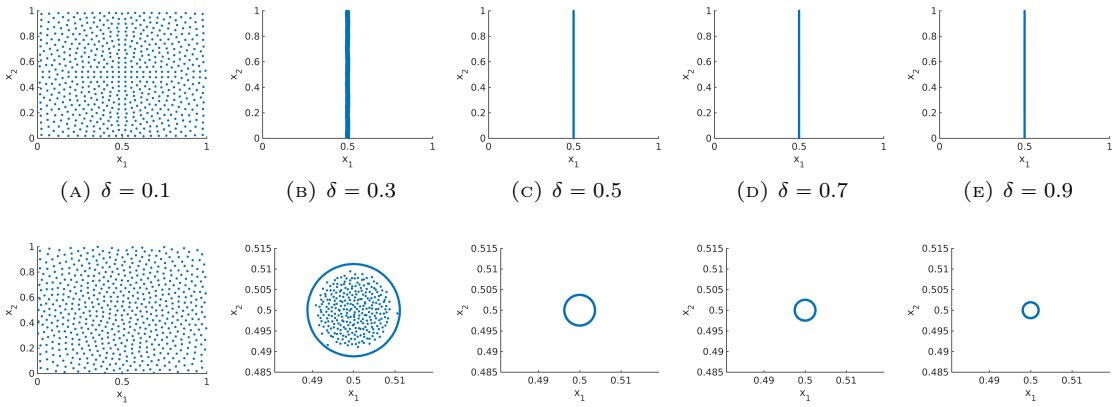

(A) $\delta = 0.1$ (B) $\delta = 0.3$ (C) $\delta = 0.5$ (D) $\delta = 0.7$ (E) $\delta = 0.9$

(F) $\delta = 0.1$ (G) $\delta = 0.3$ (H) $\delta = 0.5$ (I) $\delta = 0.7$ (J) $\delta = 0.9$

FIGURE 11. Stationary solution to the Kücken-Champod model (1.4) for force $F(d,T) = \delta F_A(d,T) + F_R(d)$ for different values of δ (i.e. different sizes of the attraction force F_A) where $\chi = 0.2$ and $\chi = 1$ (for different axis scalings) in the first and second row, respectively

4.2.9. *Dependence on the size of the repulsion force.* In this section, we consider a force of the form $F(d,T) = F_A(d,T) + \delta F_R(d)$ for $\delta \in [0,1]$ for the spatially homogeneous tensor field $T = \chi s \otimes s + l \otimes l$ with $l = (1,0)$ and $s = (0,1)$ instead of (2.1). The stationary solution to (1.4) for $\chi = 0.2$ stretches along the vertical axis as δ increases due to an additional repulsive force as illustrated in Figure 12. For $\chi = 1$, the radius of the ring pattern increases as δ, see Figure 13.

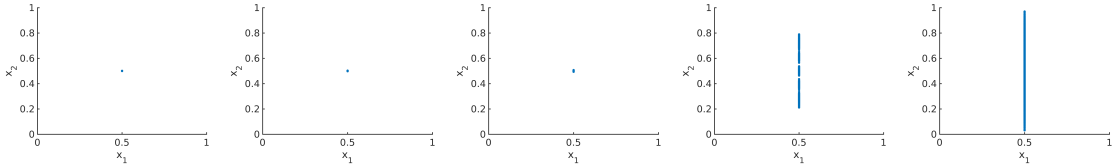

(A) $\delta = 0.1$ (B) $\delta = 0.3$ (C) $\delta = 0.5$ (D) $\delta = 0.7$ (E) $\delta = 0.9$

FIGURE 12. Stationary solution to the Kücken-Champod model (1.4) for $\chi = 0.2$ and force $F(d,T) = F_A(d,T) + \delta F_R(d)$ for different values of δ (i.e. different sizes of the repulsion force F_R)

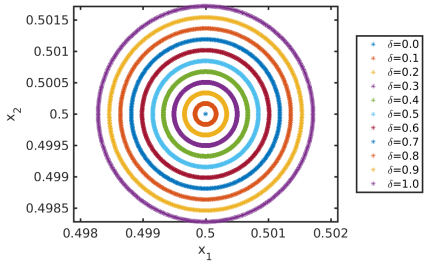

FIGURE 13. Stationary solution to the Kücken-Champod model (1.4) for $\chi = 1$ and force $F(d,T) = F_A(d,T) + \delta F_R(d)$ for different values of δ (i.e. different sizes of the repulsion force F_R)

4.2.10. *Dependence on the tensor field.* In Figures 14 and 15 the numerical solution to the Kücken-Champod model (1.4) for $N = 600$, $\chi = 0.2$ and randomly uniformly distributed data is shown for different non-homogeneous tensor fields $T = T(x)$ and different times t. Since $s = s(x)$ and $l = l(x)$ are assumed to be orthonormal vectors, the vector field $s = s(x)$ and the parameter χ determine the tensor field $T = T(x)$. One can clearly see in Figure 14 that the particles are aligned along the lines of smallest stress $s = s(x)$. However, these patterns are no equilibria. The evolution of the numerical solution for different tensor fields is illustrated in Figure 15.

In future work, the solutions to the Kücken-Champod model for non-homogeneous tensor fields $T = T(x)$ could be studied more extensively. In particular, more realistic tensor fields for the formation of fingerprint patterns could be considered. Besides, the dependence of the parameter values in the Kücken-Champod model on the resulting fingerprints could be investigated. A paper on fingerprint simulations [38] is in preparation.

4.3. Comparison of the theoretical equilibria and the numerical results. In this section, we discuss the equilibria and their stability of the N particle model (1.4) for the spatially homogeneous tensor field $T = \chi s \otimes s + l \otimes l$ with $l = (1,0)$ and $s = (0,1)$ and compare them with the numerical results.

4.3.1. *Ellipse.* In this subsection, we consider ellipse equilibria. As outlined in section **3.1** there is an additional advection along the vertical axis compared to the horizontal axis for $\chi \in [0,1)$ for the tensor field $T = \chi s \otimes s + l \otimes l$ with $l = (1,0)$ and $s = (0,1)$. This additional advection for $\chi \in [0,1)$ not only leads to an ellipse pattern stretched along the vertical axis, but also results in accumulations within the ellipse pattern, i.e. the distances of the particles are much longer along the vertical lines (e.g. at the left or right side of the ellipse) than along the horizontal lines (e.g. at the top or bottom of the ellipse). As in section **3.3** we denote the length of the minor and major axis of the ellipse state by R and $R + r$, respectively.

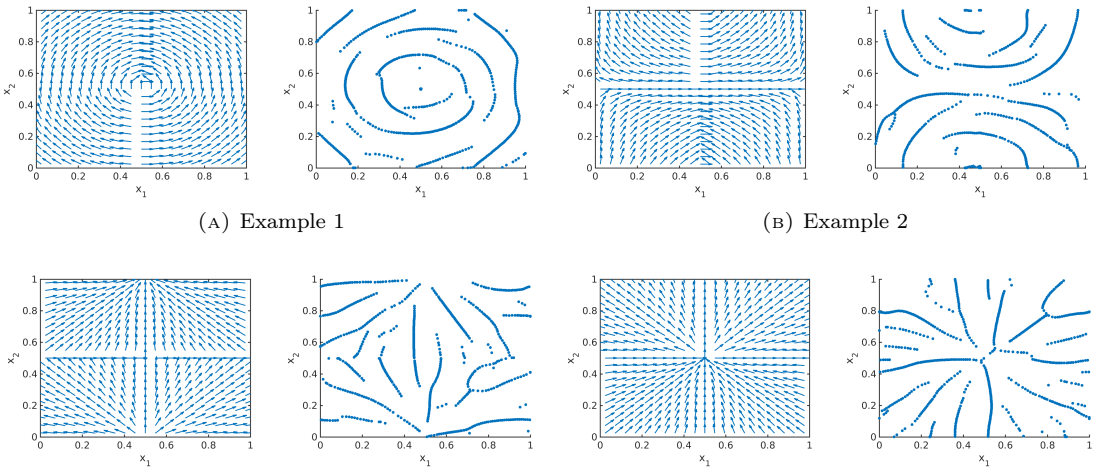

(A) Example 1 (B) Example 2

(C) Example 3 (D) Example 4

FIGURE 14. Different non-homogeneous tensor fields $T = T(x)$ given by $s = s(x)$ (left) and the numerical solution to the Kücken-Champod model (1.4) at time $t = 40000$ for $\chi = 0.2$, $T = T(x)$ and randomly uniformly distributed data (right)

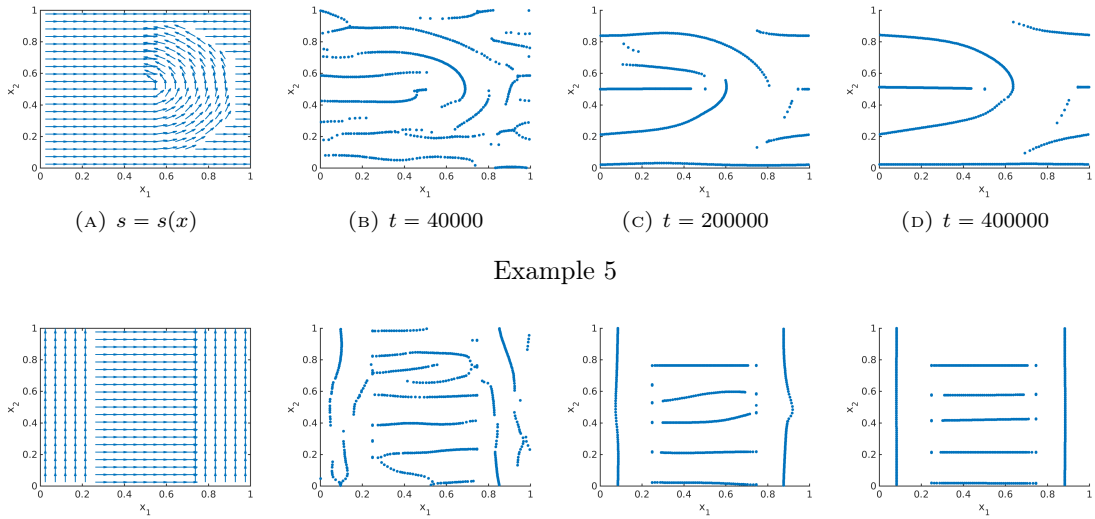

(A) $s = s(x)$ (B) $t = 40000$ (C) $t = 200000$ (D) $t = 400000$

Example 5

(E) $s = s(x)$ (F) $t = 40000$ (G) $t = 200000$ (H) $t = 400000$

Example 6

FIGURE 15. Different non-homogeneous tensor fields $T = T(x)$ given by $s = s(x)$ (left) and the numerical solution to the Kücken-Champod model (1.4) at different times t for $\chi = 0.2$, $T = T(x)$ and randomly uniformly distributed data (right)

First, we restrict ourselves to ring patterns of radius $R > 0$. We identify $\mathbb{R}^2$ with $\mathbb{C}$ and consider the ansatz

$$\bar{x}_k = \bar{x}_k(R) = x_c + R \exp\left(\frac{2\pi i k}{N}\right), \quad k = 0, \dots, N-1 \tag{4.1}$$

with center of mass x_c, i.e. the particles are uniformly distributed on a ring of radius R with center x_c. The radius $R > 0$ has to be determined such that the ansatz functions $\bar{x}_j = \bar{x}_j(R)$ satisfy

$$\sum_{\substack{k=1\\k\neq j}}^{N} F(\bar{x}_k(R) - \bar{x}_j(R), T) = 0 \tag{4.2}$$

for all $j = 0, \dots, N-1$. Let the left-hand side of (4.2) be denoted by $G_j(R)$. Note that $G_j(R)$ is highly nonlinear so that the radius R satisfying (4.2) has to be determined numerically. For $\chi = 1$, it is sufficient to consider (4.2) for $j = 0$ by symmetry arguments. Note that $\Im G_0(R) = 0$ for all $R > 0$ by the properties of F in Assumption 2.4. Hence, $R > 0$ has to be chosen such that $\Re G_0(R) = 0$. Note that the zeros of $\Re G_0$ depend on the total number of particles N. Using Newton's algorithm the unique non-trivial zero of $\Re G_0$ can be computed as $\bar{R} \approx 0.0017$ for the forces (2.5) and (2.6) in the Kücken-Champod model with parameter values from (2.7) and $N = 1200$. Hence, $\bar{R}$ is the only possible radius for ring equilibria and for $\chi = 1$, (4.1) is an equilibrium with radius $\bar{R}$. Note that this ring equilibrium has the same radius as the numerically obtained ring equilibrium in section **4.2**. Based on a linearised stability analysis [61] one can show numerically that the ring pattern is stable for $\chi = 1$ for the forces in the Kücken-Champod model for parameters in (2.7) and $N = 1200$. Since $\Im G_j(\bar{R}) = 0$ for all $j = 0, \dots, N$ for $\chi = 1$ one can easily verify that this is not true for $\chi \in [0, 1)$, i.e. there exists no radius $R > 0$ such that the ring solution (4.1) is an equilibrium for $\chi \in [0, 1)$. Note that this also coincides with the numerical results in section **4.2**.

Let us now consider the general case of an ellipse where $r \geqslant 0$. Even though an ellipse is expected to be an equilibrium it is not as straightforward as for the ring equilibrium to find suitable ansatz functions. In this section, we consider ellipse equilibria. As outlined in section **3.1** there is an additional advection along the vertical axis compared to the horizontal axis for $\chi \in [0, 1)$ for the tensor field $T = \chi s \otimes s + l \otimes l$ with $l = (1, 0)$ and $s = (0, 1)$. This additional advection not only leads to an ellipse pattern stretched along the vertical axis, but also results in accumulations within the ellipse pattern, i.e. the distances of the particles are much longer along the vertical lines (e.g. at the left or right side of the ellipse) than along the horizontal lines (e.g. at the top or bottom of the ellipse). For this reason, the particles cannot be assumed to be equidistantly distributed on the ellipse. For equiangularly distributed particles, however, the distances of the particles are longer along vertical than along horizontal lines so that one can identify $\mathbb{R}^2$ with $\mathbb{C}$ and regard the equiangular ansatz

$$\bar{x}_k = \bar{x}_k(r, R) = x_c + R\cos\left(\frac{2\pi k}{N}\right) + i(R + r)\sin\left(\frac{2\pi k}{N}\right), \quad k = 0, \dots, N-1, \tag{4.3}$$

as a good approximation. Note that an ellipse equilibrium has to satisfy

$$\sum_{\substack{k=1\\k\neq j}}^{N} F(\bar{x}_k(R, r) - \bar{x}_j(R, r), T) = 0 \tag{4.4}$$

for all $j = 0, \dots, N-1$. Let the left-hand side of (4.4) be denoted by $G_j((R, r))$. The tuples (R, r) satisfying $\Re G_j(R, r) = 0$ can be determined numerically and can be regarded as possible equilibria to (1.4). Note that the tuples (R, r) depend on N. For the force coefficients (2.5) and (2.6) in the Kücken-Champod model for parameter values (2.7) and $N = 1200$, one can observe that the larger r, the smaller R, i.e. as r increases the ring of radius R evolves into an ellipse whose major axis of length $2(R + r)$ gets longer and whose minor axis of length $2R$ gets shorter as r increases. Besides, it follows from plugging the definition of the total force for spatially homogeneous tensor fields into (4.4) that each tuple (R, r) can be associated to an equilibrium for at most one value of χ. Further note that by section **3.1** the additional advection along the vertical axis is the stronger the smaller the value of χ, implying that r increases as χ decreases. Hence, we can conclude that for a given value of χ there exists at most one tuple (R, r) such that the ansatz (4.3) is an equilibrium to (1.4). This can also be justified by evaluating $\Im G_{N/4}(R, r)$ as a function of radius pairs (R, r)

for fixed values of χ for $N = 1200$ particles. Note that these observations are consistent with the numerical results in section **4.2**.

4.3.2. *Single straight vertical line.* In this section we consider line patterns as equilibria. Because of the observations in section **3.1**, we consider vertical lines. By identifying $\mathbb{R}^2$ with $\mathbb{C}$, we make the ansatz

$$\bar{x}_k = x_c + i\frac{2k-1}{2N}, \quad k = 0, \dots, N-1, \tag{4.5}$$

for a single straight vertical line with the center of mass x_c. One can easily show that ansatz (4.5) defines an equilibrium of (1.4) for all values $\chi \in [0,1]$ by using the properties of the forces in Assumptions 2.4 and the minimum image criterion. Note that the minimum image criterion is crucial to guarantee that (4.5) is an equilibrium for even values of N. Based on a linearised stability analysis [61] one can show that (4.5) is a stable equilibrium of (1.4) for $N = 1200$ for $\chi \in [0, 0.27]$ which is consistent with the numerical results in section **4.2**.

Acknowledgments

MB acknowledges support by ERC via Grant EU FP 7 - ERC Consolidator Grant 615216 LifeInverse and by the German Science Foundation DFG via EXC 1003 Cells in Motion Cluster of Excellence, Münster, Germany. BD has been supported by the Leverhulme Trust research project grant 'Novel discretisations for higher-order nonlinear PDE' (RPG-2015-69). LMK was supported by the UK Engineering and Physical Sciences Research Council (EPSRC) grant EP/L016516/1. CBS acknowledges support from Leverhulme Trust project on Breaking the non-convexity barrier, EPSRC grant Nr. EP/M00483X/1, the EPSRC Centre Nr. EP/N014588/1 and the Cantab Capital Institute for the Mathematics of Information. The authors would like to thank Carsten Gottschlich and Stephan Huckemann for introducing them to the Kücken-Champod model and for very useful discussions on the dynamics required for simulating fingerprints.

Appendix A. Detailed computations of section 3.2

Remark A.1. Let $\tilde{T} = \chi \tilde{s} \otimes \tilde{s} + \tilde{l} \otimes \tilde{l}$ denote a spatially homogeneous tensor field for orthonormal vectors $\tilde{l}, \tilde{s} \in \mathbb{R}^2$ and set $l = (1,0)$ and $s = (0,1)$. Then,

$$\tilde{s} = R_\vartheta s \quad \text{and} \quad \tilde{l} = R_\vartheta l \tag{A.1}$$

where the angle of rotation ϑ and the corresponding rotation matrix R_ϑ are given by

$$\vartheta = \begin{cases} \arccos(\tilde{s}_2) & \tilde{s}_1 < 0 \\ 2\pi - \arccos(\tilde{s}_2) & \tilde{s}_1 > 0 \end{cases} \tag{A.2}$$

and

$$R_\vartheta = \begin{pmatrix} \cos(\vartheta) & -\sin(\vartheta) \\ \sin(\vartheta) & \cos(\vartheta) \end{pmatrix}, \tag{A.3}$$

respectively, and $\tilde{T}$ is diagonalizable with $\tilde{T} = R_\vartheta T R_\vartheta^T$ with $T = \chi s \otimes s + l \otimes l$.

Let $x_j = x_j(t)$, $j = 1, \dots, N$, denote the solution to the microscopic model (1.4) on $\mathbb{R}^2$ for the tensor field T and define

$$\tilde{x}_j(t) = x_c + R_\vartheta(x_j(t) - x_c), \quad j = 1, \dots, N$$

where x_c denotes the center of mass. Then, $\tilde{x}_j = \tilde{x}_j(t)$, $j = 1, \dots, N$, is a solution to the microscopic model (1.4) on $\mathbb{R}^2$ for the tensor field $\tilde{T}$. Besides, given an equilibrium $\bar{x}_j$, $j = 1, \dots, N$, to (1.4) on $\mathbb{R}^2$ for the tensor field T, then

$$\bar{\tilde{x}}_j = x_c + R_\vartheta(\bar{x}_j - x_c), \quad j = 1, \dots, N,$$

is an equilibrium to (1.4) on $\mathbb{R}^2$ for the tensor field $\tilde{T}$.

We show that $\tilde{x}_j,\ j=1,\dots,N$, solves (1.4) for the tensor field $\tilde{T}$. Since $x_j,\ j=1,\dots,N$, solves (1.4) for the tensor field T, we have

$$\frac{\mathrm{d}x_j}{\mathrm{d}t} = \sum_{k\neq j} f_A(|x_j-x_k|)\left[\chi\left(s\cdot(x_j-x_k)\right)s + \left(l\cdot(x_j-x_k)\right)l\right] + f_R(|x_j-x_k|)(x_j-x_k)$$

for all $j=1,\dots,N$ by Remark 2.7. Note that $\tilde{x}_j-\tilde{x}_k = R_\vartheta(x_j-x_k)$ and $|\tilde{x}_j-\tilde{x}_k| = |x_j-x_k|$. Using (A.1) as well as the fact that R_ϑ is an orthogonal matrix we get

$$\chi\left(\tilde{s}\cdot(\tilde{x}_j-\tilde{x}_k)\right)\tilde{s} + \left(\tilde{l}\cdot(\tilde{x}_j-\tilde{x}_k)\right)\tilde{l} = R_\vartheta\left[\chi\left(s\cdot(x_j-x_k)\right)s + \left(l\cdot(x_j-x_k)\right)l\right].$$

This implies

$$\frac{\mathrm{d}\tilde{x}_j}{\mathrm{d}t} = \sum_{k\neq j} f_A(|\tilde{x}_j-\tilde{x}_k|)\left[\chi\left(\tilde{s}\cdot(\tilde{x}_j-\tilde{x}_k)\right)\tilde{s} + \left(\tilde{l}\cdot(\tilde{x}_j-\tilde{x}_k)\right)\tilde{l}\right] + f_R(|\tilde{x}_j-\tilde{x}_k|)(\tilde{x}_j-\tilde{x}_k)$$

for all $j=1,\dots,N$, i.e. $\tilde{x}_j,\ j=1,\dots,N$, solves (1.4) for the tensor field $\tilde{T}$. Similarly, one can show that $\bar{\tilde{x}}_j$ is an equilibrium to (1.4) for the tensor field $\tilde{T}$, given that $\bar{x}_j,\ j=1,\dots,N$, is an equilibrium to (1.4) for the tensor field T.

Remark A.2. Let $\tilde{T} = \chi\tilde{s}\otimes\tilde{s} + \tilde{l}\otimes\tilde{l}$ denote a spatially homogeneous tensor field for orthonormal vectors $\tilde{l},\tilde{s}\in\mathbb{R}^2$. Given $l=(1,0)$, $s=(0,1)$ and angle of rotation ϑ in (A.2), then $\tilde{T} = R_\vartheta T R_\vartheta^T$ with $T = \chi s\otimes s + l\otimes l$. Let $\rho=\rho(\mathrm{d}x)$ denote an equilibrium state to the mean-field PDE (2.8) on $\mathbb{R}^2$ for the tensor field T and define

$$\tilde{\rho}(x) = \rho\left(x_c + R_\vartheta^{-1}(x-x_c)\right) \text{ a.e.} \tag{A.4}$$

where R_ϑ is the rotation matrix (A.3) and x_c denotes the center of mass. Then, $\tilde{\rho}$ is an equilibrium state to (2.8) for the tensor field $\tilde{T}$.

To show this result note that for $x\in\mathbb{R}^2$ we have

$$\begin{aligned}
&\left(F(\cdot,T)*\tilde{\rho}\right)\left(x_c+R_\vartheta(x-x_c)\right)\\
&= \int_{\mathbb{R}^2} F\left(x_c+R_\vartheta(x-x_c)-\left(x_c+R_\vartheta(x-x_c')\right),\tilde{T}\right)\rho(\mathrm{d}x')\\
&= \int_{\mathbb{R}^2}\Big[f_R(|x-x'|)R_\vartheta(x-x')\\
&\qquad\qquad + f_A(|x-x'|)\left[\chi\left(\tilde{s}\cdot(R_\vartheta(x-x'))\right)\tilde{s} + \left(\tilde{l}\cdot(R_\vartheta(x-x'))\right)\tilde{l}\right]\Big]\rho(\mathrm{d}x')\\
&= R_\vartheta\left(F(\cdot,T)*\rho\right)(x)
\end{aligned}$$

where the first equality follows from (A.4) and the substitution rule. The definitions of the repulsion and attraction forces in (2.2) and (2.3) are used in the second equality and (A.1) is inserted in the third equality. Since $x\in\mathrm{supp}(\tilde{\rho})$ implies $x\in\mathrm{supp}(\rho(x_c+R_\vartheta^{-1}(\cdot-x_c)))$ and $\left(F(\cdot,T)*\tilde{\rho}\right)(x) = R_\vartheta\left(F(\cdot,T)*\rho\right)\left(x_c+R_\vartheta^{-1}(x-x_c)\right)$, $\tilde{\rho}$ is an equilibrium state to (2.8) for the tensor field $\tilde{T}$ provided that ρ is an equilibrium state to (2.8) for the tensor field T.

References

[1] G. Albi, D. Balagué, J. A. Carrillo, and J. von Brecht. Stability analysis of flock and mill rings for second order models in swarming. *SIAM J. Appl. Math.*, 74(3):794–818, 2014.

[2] L. A. Ambrosio, N. Gigli, and G. Savaré. *Gradient flows in metric spaces and in the space of probability measures*. Lectures in Mathematics. Birkhäuser, 2005.

[3] D. Balagué, J. A. Carrillo, T. Laurent, and G. Raoul. Dimensionality of local minimizers of the interaction energy. *Archive for Rational Mechanics and Analysis*, 209(3):1055–1088, 2013.

[4] D. Balagué, J. A. Carrillo, T. Laurent, and G. Raoul. Nonlocal interactions by repulsive-attractive potentials: radial ins/stability. *Physica D: Nonlinear Phenomena*, 260:5–25, 2013.

[5] D. Balagué, J. A. Carrillo, and Y. Yao. Confinement for repulsive-attractive kernels. *Disc. Cont. Dyn. Sys.-B*, 19:1227–1248, 2014.

[6] P. Ball. *Nature's patterns: A tapestry in three parts*. Oxford University Press, 2009.

[7] A. J. Bernoff and C. M. Topaz. A primer of swarm equilibria. *SIAM J. Appl. Dyn. Syst.*, 10:212–250, 2011.

[8] A. Bertozzi, J. Garnett, and T. Laurent. Characterization of radially symmetric finite time blowup in multidimensional aggregation equations. Preprint.
[9] A. L. Bertozzi, J. A. Carrillo, and T. Laurent. Blow-up in multidimensional aggregation equations with mildly singular interaction kernels. *Nonlinearity*, 22(3):683, 2009.
[10] A. L. Bertozzi, J. B. Garnett, and T. Laurent. Characterization of radially symmetric finite time blowup in multidimensional aggregation equations. *SIAM J. Math. Anal.*, 44(2):651–681, 2012.
[11] A. L. Bertozzi and T. Laurent. Finite-time blow-up of solutions of an aggregation equation in $\mathbb{R}^n$. *Communications in Mathematical Physics*, 274(3):717–735, 2007.
[12] A. L. Bertozzi, T. Laurent, and F. Léger. Aggregation and spreading via the newtonian potential: The dynamics of patch solutions. *Mathematical Models and Methods in Applied Sciences*, 22(supp01):1140005, 2012.
[13] A. L. Bertozzi, H. Sun, T. Kolokolnikov, D. Uminsky, and J. H. Von Brecht. Ring patterns and their bifurcations in a nonlocal model of biological swarms. Preprint.
[14] B. Birnir. An ode model of the motion of pelagic fish. *Journal of Statistical Physics*, 128(1):535–568, 2007.
[15] A. Blanchet, V. Calvez, and J. A. Carrillo. Convergence of the mass-transport steepest descent scheme for the subcritical patlak–keller–segel model. *SIAM Journal on Numerical Analysis*, 46(2):691–721, 2008.
[16] A. Blanchet, J. Dolbeault, and B. Perthame. Two-dimensional keller-segel model: Optimal critical mass and qualitative properties of the solutions. *Electronic Journal of Differential Equations (EJDE)*, 2006:Paper No. 44, 33 p., 2006.
[17] S. Boi, V. Capasso, and D. Morale. Modeling the aggregative behavior of ants of the species polyergus rufescens. *Nonlinear Analysis: Real World Applications*, 1(1):163 – 176, 2000.
[18] M. Burger, V. Capasso, and D. Morale. On an aggregation model with long and short range interactions. *Nonlinear Analysis: Real World Applications*, 8(3):939–958, 2007.
[19] M. Burger and M. DiFrancesco. Large time behavior of nonlocal aggregation models with nonlinear diffusion. *Networks and Heterogeneous Media*, 3(4):749–785, 2008.
[20] S. Camazine, J.-L. Deneubourg, N. R. Franks, J. Sneyd, G. Theraulaz, and E. Bonabeau. Self-organization in biological systems. *Princeton Univ. Press, Princeton*, 2003.
[21] J. A. Cañizo, J. A. Carrillo, and Francesco S. Patacchini. Existence of compactly supported global minimisers for the interaction energy. *Archive for Rational Mechanics and Analysis*, 217(3):1197–1217, 2015.
[22] A. J. Carrillo, J. R. McCann, and C. Villani. Contractions in the 2-wasserstein length space and thermalization of granular media. *Archive for Rational Mechanics and Analysis*, 179(2):217–263, 2006.
[23] J. A. Carrillo, A. Chertock, and Y. Huang. A finite-volume method for nonlinear nonlocal equations with a gradient flow structure. *Communications in Computational Physics*, 17(1):233–258, 11 2014.
[24] J. A. Carrillo, M. Chipot, and Y. Huang. On global minimizers of repulsive–attractive power-law interaction energies. *Philosophical Transactions of the Royal Society of London A: Mathematical, Physical and Engineering Sciences*, 372(2028), 2014.
[25] J. A. Carrillo, M. G. Delgadino, and A. Mellet. Regularity of local minimizers of the interaction energy via obstacle problems. *Communications in Mathematical Physics*, 343(3):747–781, 2016.
[26] J. A. Carrillo, M. Di Francesco, A. Figalli, T. Laurent, and D. Slepčev. Global-in-time weak measure solutions and finite-time aggregation for nonlocal interaction equations. *Duke Math. J.*, 156(2):229–271, 02 2011.
[27] J. A. Carrillo, L. C. F. Ferreira, and J. C. Precioso. A mass-transportation approach to a one dimensional fluid mechanics model with nonlocal velocity. *Advances in Mathematics*, 231(1):306 – 327, 2012.
[28] J. A. Carrillo, A. Figalli, and F. S. Patacchini. Geometry of minimizers for the interaction energy with mildly repulsive potentials. Preprint.
[29] J. A. Carrillo, M. Fornasier, J. Rosado, and G. Toscani. Asymptotic flocking dynamics for the kinetic cucker–smale model. *SIAM Journal on Mathematical Analysis*, 42(1):218–236, 2010.
[30] J. A. Carrillo and Y. Huang. Explicit equilibrium solutions for the aggregation equation with power-law potentials. to appear in Kinetic Rel. Mod.
[31] J. A. Carrillo, F. James, F. Lagoutière, and N. Vauchelet. The filippov characteristic flow for the aggregation equation with mildly singular potentials. *J. Differential Equations*, 260:304–338, 2016.
[32] J.A. Carrillo, M. Di Francesco, A. Figalli, T. Laurent, and D. Slepčev. Confinement in nonlocal interaction equations. *Nonlinear Analysis: Theory, Methods and Applications*, 75(2):550 – 558, 2012.
[33] J.A. Carrillo, F. James, F. Lagoutière, and N. Vauchelet. The filippov characteristic flow for the aggregation equation with mildly singular potentials. *Journal of Differential Equations*, 260(1):304 – 338, 2016.
[34] J.A. Carrillo, R. J. McCann, and C. Villani. Kinetic equilibration rates for granular media and related equations: entropy dissipation and mass transportation estimates. *Revista Matematica Iberoamericana*, 19:971–1018, 2003.
[35] K. Craig and A. L. Bertozzi. A blob method for the aggregation equation. *Math. Comput.*, 85(300), 2016.
[36] P. Degond and S. Motsch. Large scale dynamics of the persistent turning walker model of fish behavior. *Journal of Statistical Physics*, 131:989–1021, 2008.
[37] A M. Delprato, A. Samadani, A. Kudrolli, and L. S. Tsimring. Swarming ring patterns in bacterial colonies exposed to ultraviolet radiation. *Phys. Rev. Lett.*, 87, 2001.
[38] B. Düring, C. Gottschlich, S. Huckemann, L. Kreusser, and C.-B. Schönlieb. Study of an anisotropic particle model for simulating fingerprints. in preparation.
[39] M. R. D'Orsogna, Y. L. Chuang, A. L. Bertozzi, and L. S. Chayes. Self-propelled particles with soft-core interactions: Patterns, stability, and collapse. *Phys. Rev. Lett.*, 96, 2006.

[40] L. Edelstein-Keshet, J. Watmough, and D. Grunbaum. Do travelling band solutions describe cohesive swarms? an investigation for migratory locusts. *J. Math. Bio.*, 36:515–549, 1998.
[41] F. Ercolessi. A molecular dynamics primer. Spring College in Computational Physics, ICTP, 1997.
[42] K. Fellner and G. Raoul. Stable stationary states of non-local interaction equations. *Mathematical Models and Methods in Applied Sciences*, 20(12):2267–2291, 2010.
[43] K. Fellner and G. Raoul. Stability of stationary states of non-local equations with singular interaction potentials. *Mathematical and Computer Modelling*, 53(7–8):1436 – 1450, 2011. Mathematical Methods and Modelling of Biophysical Phenomena.
[44] R.C. Fetecau, Y. Huang, and T. Kolokolnikov. Swarm dynamics and equilibria for a nonlocal aggregation model. *Nonlinearity*, 24:2681–2716, 2011.
[45] F. Golse. *Macroscopic and Large Scale Phenomena: Coarse Graining, Mean Field Limits and Ergodicity*, chapter On the Dynamics of Large Particle Systems in the Mean Field Limit, pages 1–144. Springer International Publishing, Cham, 2016.
[46] M.K. Irmak. Multifunctional merkel cells: their roles in electromagnetic reception, fingerprint formation, reiki, epigenetic inheritance and hair form. *Med. Hypotheses*, 75:162–168, 2010.
[47] D.-K. Kim and K. A. Holbrook. The appearance, density, and distribution of merkel cells in human embryonic and fetal skin: Their relation to sweat gland and hair follicle development. *Journal of Investigative Dermatology*, 104(3):411 – 416, 1995.
[48] T. Kolokolnikov, H. Sun, D. Uminsky, and A. L. Bertozzi. Stability of ring patterns arising from two-dimensional particle interactions. *Phys. Rev. E*, 84(1):015203, Jul 2011.
[49] M. Kücken and C. Champod. Merkel cells and the individuality of friction ridge skin. *Journal of Theoretical Biology*, 317:229 – 237, 2013.
[50] M. Kücken and A. Newell. A model for fingerprint formation. *Europhysics Letters*, 68:141–146, 2004.
[51] M. Kücken and A. Newell. Fingerprint formation. *Journal of Theoretical Biology*, 235:71–83, 2005.
[52] T. Laurent. Local and global existence for an aggregation equation. *Communications in Partial Differential Equations*, 32:1941–1964, 2007.
[53] H. Li and G. Toscani. Long-time asymptotics of kinetic models of granular flows. *Archive for Rational Mechanics and Analysis*, 172(3):407–428, 2004.
[54] A. Mogilner and L. Edelstein-Keshet. A non-local model for a swarm. *J. Math. Biol.*, 38:534–570, 1999.
[55] A. Mogilner, L. Edelstein-Keshet, L. Bent, and A. Spiros. Mutual interactions, potentials, and individual distance in a social aggregation. *Journal of Mathematical Biology*, 47(4):353–389, 2003.
[56] A. Okubo and S.A. Levin. *Interdisciplinary Applied Mathematics: Mathematical Biology*, chapter Diffusion and Ecological Problems, page 197–237. Springer, New York, 2001.
[57] J. K. Parrish and L. Edelstein-Keshet. Complexity, pattern, and evolutionary trade-offs in animal aggregation. *Science*, 284:99–101, 1999.
[58] I. Prigogine and I. Stenger. *Order out of Chaos*. Bantam Books, New York, 1984.
[59] G. Raoul. Non-local interaction equations: Stationary states and stability analysis. *Differential Integral Equations*, 25:417–440, 2012.
[60] C. M. Topaz and A. L. Bertozzi. Swarming patterns in a two-dimensional kinematic model for biological groups. *SIAM J. Appl. Dyn. Syst.*, 65:152–174, 2004.
[61] A. M. Turing. The chemical basis of morphogenesis. *Philosophical Transactions of the Royal Society (B)*, 237:37–72, 1952.
[62] C. Villani. *Topics in optimal transportation*. Graduate studies in mathematics. American Mathematical Society, cop., Providence (R.I.), 2003.
[63] J. von Brecht, D. Uminsky, T. Kolokolnikov, and A. L. Bertozzi. Predicting pattern formation in particle interactions. *Mathematical Models and Methods in Applied Sciences*, 22(supp01):1140002, 2012.
[64] J. H. von Brecht and D. Uminsky. On soccer balls and linearized inverse statistical mechanics. *Journal of Nonlinear Science*, 22(6):935–959, 2012.
[65] L. Wu and D. Slepčev. Nonlocal interaction equations in environments with heterogeneities and boundaries. *Communications in Partial Differential Equations*, 40(7):1241–1281, 2015.